Integrated Geophysical Analysis for the presence of Gas Hydrates in Blake Ridge, Offshore, South Carolina, USA.

By

Ahmed Rafeh

MPHIL Geophysics

(2021-2023)

DEPARTMENT OF EARTH SCIENCES

QUAID-I-AZAM UNIVERSITY

ISLAMABAD

To start with the greatest name of Almighty Allah. The Most gracious and merciful, with Him is the knowledge of the Hour, He sends down the rain, and knows that which is in the wombs. No person knows what he will earn tomorrow, and no person knows in what land he will die. The knower of the unseen is Allah these are the keys of the unseen, whose knowledge Allah alone has kept for himself and no one else knows them unless Allah tells him about them.

DEDICATION

I would like to dedicate this thesis work to my parents, their love, encouragement, guidance and prays make me able to achieve such success and honor.

Acknowledgement

In the name of Allah Almighty, the most Gracious, the most Compassionate. Almighty, on whom ultimately, we depend for sustenance and guidance. I bear witness that Hazrat Muhammad (SAWW) is the last messenger, whose life is role model for the whole mankind till the Day of Judgment. I thank Allah Almighty for giving me strength and skill to finalize this study.

I would like to manifest my appreciation to my Supervisor Dr. Shazia Naseem and express my sincerest appreciation for her guidance in the preparation of this thesis. She helped me in all aspects of work.

I also thank the whole faculty of my department for providing me with an academic base, which has enabled me to take up this study I pay my thanks to the employees of clerical office who helped me a lot and all those their names do not appear here who have contributed to the successful completion of this study. I acknowledge that department has provided me necessary softwares to complete my study.

I acknowledge my friends especially Yawar Amin, Chaudhary Umer Ghaffar, Farmanullah Khan Khattak and Muhammad Aftab Shabir who helped me in my work.

Ahmed Rafeh

February, 2023

ABSTRACT

Gas hydrates contain a major untapped source of energy and are of potential economic importance. The Blake Ridge is one of the largest passive margins of gas hydrate provinces on Earth. The Blake Ridge Diapir is the southernmost of a line of salt diapirs along the Carolina trough. Gas hydrates are supposed to be present on the crest of the Blake Ridge.

Identification and quantification of gas-hydrate and free-gas reservoirs in unconsolidated sediments using seismic data are important because the seismic method is the most promising remote sensing technique for the delineation of such prospects. Analysis of three-dimensional (3D) seismic data has led to significant advances in our understanding of the distribution of gas hydrates on the Blake Ridge. The most significant observation is a thick zone of gas hydrates. Bottom-simulating reflector (BSR) is observed as the base of the Gas Hydrates Stability Zone (GHSZ). BSR is not continuous throughout, and that can be explained by low methane supply rates or gas seeps.

Seismic attribute analysis, seismic interpretation, petrophysics, inversion, Lambda-Mu-Rho (LMR) inversion, porosity section, and saturation results support the presence of gas hydrates. Amplitude blanking is also observed above BSR, which is a typical indication of gas hydrates. The porosity section was calculated using the cross-plot method, while saturation was derived from probabilistic neural network (PNN).

Table of Contents

Chapter 1

Introduction of Gas Hydrates

Gas hydrates are crystalline solids composed of water molecules and a gas, most often methane, encased in a crystal lattice (Sloan, 1990). Gas hydrates are crystalline complexes made of water and any of the following light molecules: methane, ethane, propane, iso-butane, regular butane, nitrogen, carbon dioxide, and hydrogen sulphide. It is generally known that other polar compounds with diameters between those of argon (0.35 nm) and ethyl cyclohexane (0.9–1) may also form hydrates. Generally, hydrate formation occurs when water molecules are present in close proximity to molecules that are either above or below the freezing point and when pressures are quite high. These host molecules are encompassed by water molecules, which form stable cage-like structures (Aregbe, 2017).

1.1 Formation and accumulation of Gas Hydrates

Crystalline compounds called natural gas hydrates, sometimes referred to as gas hydrates, are produced when methane gas and water molecules coexist at the appropriate pressure and temperature. When subjected to high pressure and temperatures that are either just above or just below 0 degree Celsius, methane hydrate may remain stable. Nevertheless, large amounts of hydrate are formed at the continental shelf as a result of the impact of the geothermal gradient (Rempel and Buffett, 1997). This is the case even though the pressure and temperature of the majority of ocean settings offer conditions that are suitable for the stability of methane hydrate. The geothermal gradient makes it possible for temperatures at certain depths to be higher than the temperature at which equilibrium is reached at the in-situ pressure. This makes methane hydrate stable. The formation of a structure resembling a cage is kept stable by the interactions that take place between the molecules of water and the molecules of methane gas. These interactions lead to the production of a lattice that is relatively resilient and stable in nature. Methane gas may be stored in gas hydrates with a high capacity. One cubic meter of a typical hydrate has the ability to store around 180 standard cubic meters of methane gas when the temperature and pressure are kept at normal levels (Rempel and Buffett, 1997).

Hydrates are formed by four important factors: extremely high pressure, very low temperature, the presence of water, and the presence of methane. Due to the

massive overburden of the water above, the sub seabed environment is subjected to very high pressures. Due to the staggering quantity of organic matter deposited on the ocean floor over millions of years, the organic matter will decay and transform into natural gas. This gas will reach a zone where the pressure is high enough and the temperature is low enough to support the development of these ice-like substances as it migrates upward through several layers of sediment. Accordingly, the appropriate geothermal gradient associated with the formation will inhibit the development of hydrates below a specific depth (Kvenvolden, 1998). This depth is often referred to in seismic interpretation as the Bottom Simulating Reflector(BSR) and may be seen in seismic data as a negative impedance reflection that closely resembles the sea floor's structure (Hornbach et al., 2008; Tinivella and Lodolo, 2000; Tinivella and Accaino, 2000). Areas below the BSR are always anticipated to contain free gas and water, whereas areas above the BSR are anticipated to have methane hydrates (Haacke et al., 2007).

Most hydrate deposits are found in water deeper than 300 m. Their zones of existence range from the seafloor to a few hundred meters down, and this depends on the temperature gradient in the area. Based on research and investigation, scientists think that a lot of methane gas is stuck in the hydrate deposits and the sediments below them. The answer to an endless supply of energy is the exploration and exploitation of gas hydrate resources. This source of power is clean and good for the environment (Aregbe, 2017).

1.2Stability Conditions of Gas Hydrates

Methane hydrate is stable at low temperatures and high pressures when there is an abundance of free gas and water. Deep-sea sediments that are full of organic matter meet these conditions. The stability field of gas hydrates in deep-sea sediments is shown in figure 1.1. Conditions of three-phase equilibrium have been determined for the system consisting of methane, water, and methane hydrate, as shown by the solid curve. The temperature profile of sea water is shown by the broken line in the graph. In the ocean, the floor at a depth of 2500 meters (at a temperature of 33 degrees Celsius and a pressure of 250 bars) is well within the stability range for methane hydrate. Methane hydrate may be formed if the water at the bottom of the ocean is oversaturated with methane. On the continental slope of the Gulf of Mexico and atop the mud volcanoes of the Caspian Sea are two examples of places where the

circumstances necessary for the formation of methane seeps are present. The zone of hydrate stability is also found in the shallow burial sediments.

The temperature of the sediments rises with increasing depth until it surpasses the parameters necessary for stability at a depth of 600 Meters Below SeaFloor (mbsf). Below this depth, gas hydrates will become unstable. The Base of Gas Hydrate Stability (BGHS) is the bottom limit of gas hydrate stability. The BGHS fluctuates depending on the water depth and the thermal gradient; for example, it is between 300 and 400 mbsf at a water depth of 1000 to 2000 meters, while it is between 400 and 600 mbsf at a depth of 3000 to 4000 meters. On-land sediments underneath the permafrost in polar areas, such as Siberia, Alaska, and Arctic Canada, may also be found to have low temperatures, high pressures, and enough volumes of free hydrocarbon gases. These circumstances can be found in a variety of polar environments.

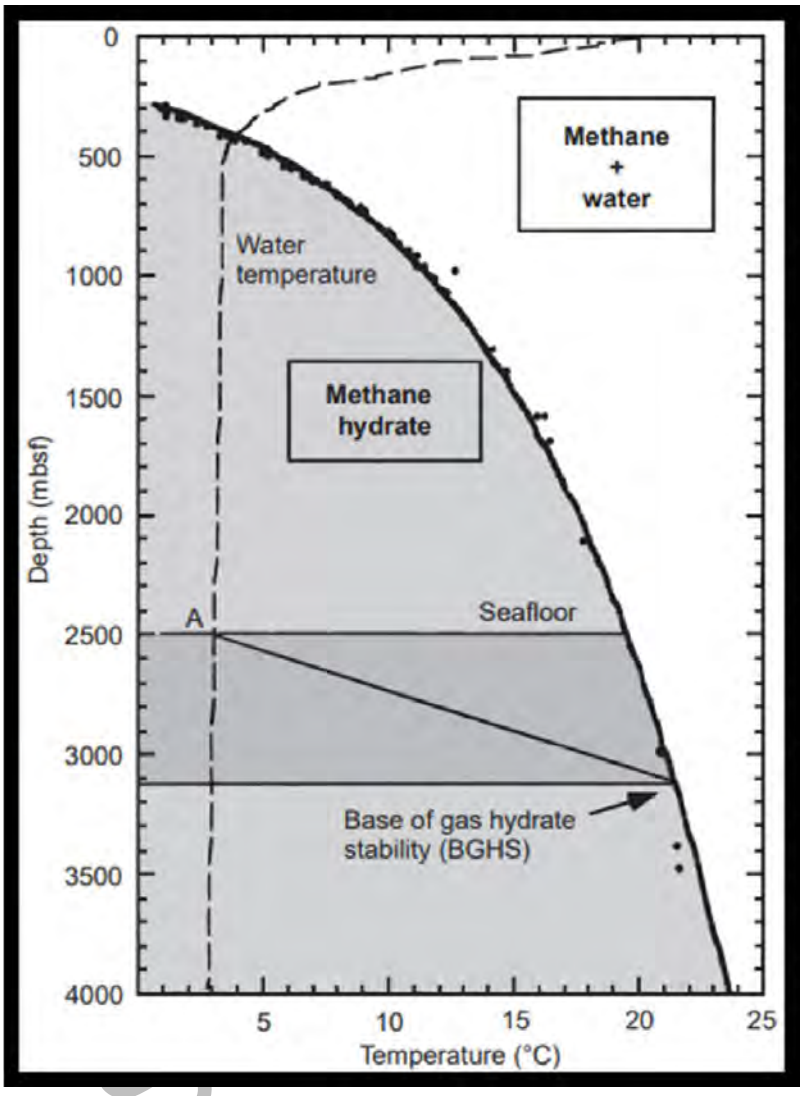

Figure 1.1 The stability conditions of methane hydrate in marine sediments. (Matsumoto, 1995.)

1.3Importance of Gas Hydrates

Natural gas, which is mostly made up of methane, is used in the industry as a fuel due to the methods that may be used to directly handle it. Both directly as a heating fuel and indirectly through the process of energy conversion, there are technologies that are easy to get and don't cost much to use. In addition to this, the ratio of hydrogen atoms to carbon atoms in methane gas is higher than in the case of other hydrocarbon fuels. This means that when methane is burned, carbon dioxide is made in smaller amounts. In addition, compared to other types of hydrocarbon fuels, such as coal and oil, methane gas is an energy source that is environmentally friendly. It is interesting to note that research has revealed that the production of carbon dioxide by methane gas is substantially lower than that of alcohols and even

significantly lower than that of liquid petroleum and fuels that come from oil (Aregbe, 2017).

The discovery and exploitation of gas hydrate reserves, which present the prospect of a practically infinite supply of methane, will surely have an influence on the expansion of the gas-based energy economy and help it surpass the oil-based energy economy (Aregbe, 2017). The availability of fuel from hydrate deposits is compared to the availability of fuel from other sources using a unit of 10^{15} g of carbon in Figure 1.2.

In recent years, hydrate production has come under the scrutiny of researchers and investigators as a possible source of renewable energy. It is believed that the amount of carbon found in gas hydrates is more than twice as much as that found in coal, conventional gas, and petroleum reserves combined (Ruffine, et al., 2010). Gas hydrate deposits hold a massive amount of energy in the form of methane gas in its purest form, which has the potential to serve as a renewable source of energy.

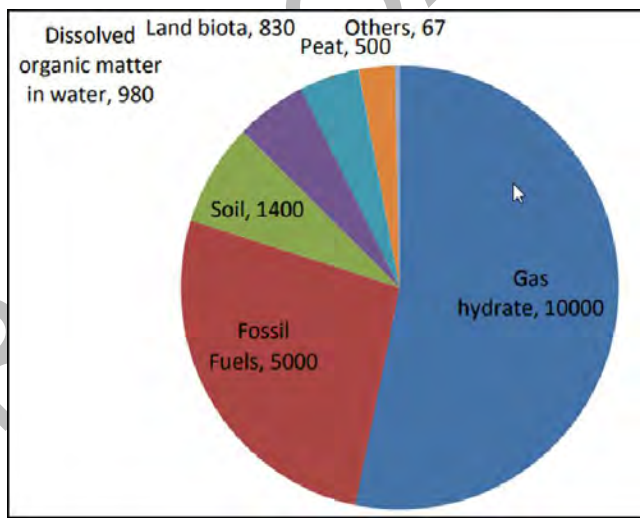

Figure 1.2 Gas hydrates deposits compared with other fuel resources, units = 10^{15} g of carbon (Tohidi, 2014)

1.4Study Area

Blake Ridge is a contourite drift that forms a portion of the Blake Plateau. This plateau is located in the mid-Atlantic, off the coast of the southeastern United States. The beaches of the four states of North Carolina, South Carolina, Georgia, and Florida are all in touch with the Blake Plateau. Blake Plateau extends for more than

100 miles in the direction of latitude, but Blake Ridge is a far more modest feature. Due to the presence of methane hydrates in this area, Blake Ridge has been given the reputation of being one of the world's most fertile and fruitful provinces of methane hydrates (Holbrook et al., 1996). The Blake Ridge is one of the best-studied methane hydrate systems on Earth.

3D seismic survey was done in year 2000. In survey 95 inlines and 1306 crosslines data was acquired. Total area of the survey was 348.93 sq.km. Inline bin size was 75 m/line and Crossline bin size was 37.5 m/line. Figure 1.3 shows satellite image of the Blake Ridge with red rectangle showing the 3D seismic data acquisition area in offshore.

Figure 1.3: The Blake Ridge system, which contains the red rectangle for which the seismic data was collected.

1.5Basemap

The base map is a crucial component of interpretation since it displays the spatial location of each seismic picket. A base map for a geophysicist is one that depicts the orientations of seismic lines and specifies the sites at which seismic data were gathered, or a map that consists of a certain number of inlines and crosslines on

which a seismic survey is being conducted. The position of lease and concession boundaries, wells, seismic survey stations, and other cultural data like buildings and roads are often shown on a base map, along with geographic coordinates such as latitude and longitude.

3D seismic basemap showing orientation of the survey acquired at Blake Ridge with 95 inlines and 1306 crosslines is shown in figure 1.4.

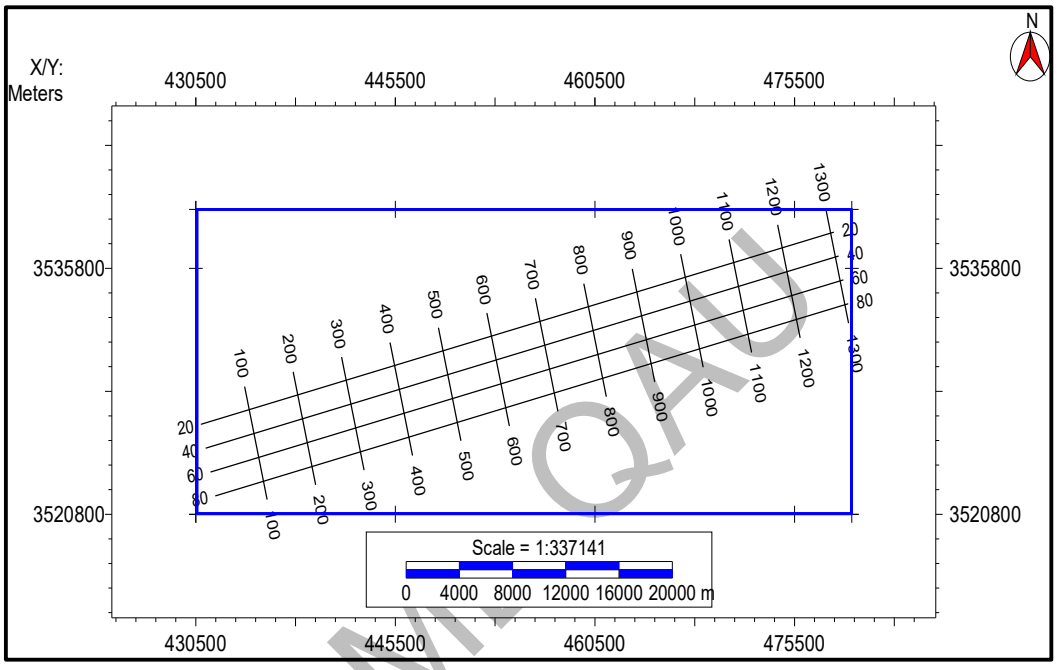

Figure 1.4 Basemap of study area.

1.6Methodology

Blake Ridge is one of the extensive studied areas for the understanding of Gas Hydrates. 3D data is used for this purpose as 3D data shows the extension of every event in all directions. The objective of this study is to understand the basics of Gas Hydrates and to get spatial extent of well log data and other reservoir parameters on seismic scale.

To understand the mechanism of Gas Hydrates in Blake Ridge province interpretation on 3D seismic is done. For the interpretation of BSR attribute analysis is considered. Different attributes are applied to check the position of BSR. BSR is marked and time contour map is generated. Also Seabed is marked as it is the first reflection seen on seismic data.

Amplitude Blanking is a typical feature of Gas Hydrates as there is not a large impedance contrast in Gas Hydrates stability zone (GHSZ). Amplitude Blanking is observed on seismic as well as from attribute sections of seismic. Log analysis is done, and results support the presence of Gas Hydrates.

Seismic Inversion analysis is a process to get reservoir parameters on seismic scale. Inverted P and S-Impedance volumes are calculated by Model Base Inversion. By using these inverted volumes different parameters are estimated on the seismic. Lambda-Mu-Rho (LMR) is estimated by using both P and S-impedance volumes. Porosity is estimated with help of cross plot method. Hydrate saturation is estimated on the seismic scale by probabilistic neural network (PNN).

Softwares used are Hampson Russel Software (HRS) and Kingdom 2021. For the writing of thesis Microsoft Word is used.

Chapter 2

Geology and Tectonics

A linear array of at least 25 diapirs that stretches northeastward along the seaward edge of the Carolina Trough is terminated by the Blake Ridge diapir, which is the southernmost of the diapirs in the array (Dillon et al., 1983; Dillon and Popenoe, 1988). The Carolina Trough is one of the four primary continental margin basins that were produced because of the original rifting that occurred along the Atlantic border of the United States. It is a long, narrow basin that is about 450 kilometers long and 40 kilometers wide. However, a significant amount of salt has flowed seaward under the weight of basin fill and formed the diapirs that rise along the seaward edge of the deep basin, which is defined by the East Coast Magnetic Anomaly. This salt remains in the basin at a tremendous depth of roughly 11 kilometers. Several still-active growth faults have been established along the landward side of the basin's deepest portion as a result of the subsidence that was caused by the migration of salt. The diapir emerges close to the landward end of the Blake Ridge, which is an actively accreting and migrating sediment drift deposit. The Blake Ridge is in the transition zone between the carbonate platform of the Blake Plateau/Bahamas and the clastic-dominated eastern continental margin of the United States (Dillon and Popenoe, 1988). Based on significant chloride content in samples of interstitial fluids taken from sediments located above the diapir, it is hypothesized that the diapir was formed because of salt coming up from a depth in the Carolina Trough (Dillon et al., 1983; Paull et al., 1996). Photographs obtained near the peak of the Blake Ridge Diapir provide evidence of the existence of chemosynthetic communities, in addition to authigenic carbonates, which were most likely produced by the oxidation of methane by the surrounding salt water (Esikov and Pashkina, 1990; Paull et al., 1996). Pockmarks on the ocean bottom may be shown, on high-resolution seismic profiles, to be the source of plumes that rise into the water column (Paull et al., 1995). Furthermore, Egeberg (2000) studied the interstitial waters from ODP Drill site 996 (Paull et al., 1996) and, using transport equations for pore-water Cl^- and δ^2H, determined that a transport-dominated system is the most effective method for explaining the high concentrations of hydrate at the seabed.

Gas hydrates, carbonate accumulations, and hydrocarbon seeps comparable to those reported at ODP Site 996 have been discovered in several places around continental margins, in areas where methane-rich fluids are venting onto the seabed (Holvland and Judd, 1988; Esikov and Pashkina, 1990; Hovland, 1992; Paull et al., 1996; Ginsburg and Soloviev, 1997; Soloviev and Ginsburg, 1997).

According to both experimental observations (Brewer et al., 1997) and theoretical considerations (Ruppel, 1997), the distribution of gas hydrate appears to be largely controlled by lithology and, in particular, the size of the pore spaces between sediment grains. These findings were published in the same year. The Blake Ridge is about 350 km off the coast of South Carolina (Figure 2.1). It is a large drift deposit where gas hydrate is found in wide areas (Dillon and Paull, 1983). The geology and topography on the crest of Blake Ridge are not particularly complex. However, the sediment that was recovered on Leg 164 presents a once-in-a-lifetime opportunity to investigate the fundamental characteristics of hydrated sediment and to comprehend the ways in which variations in hydrate distribution are influenced by lithological, chemical, and hydrological factors.

The drill sites demonstrate that the Blake Ridge is a significant Neogene and Quaternary sediment drift made up of hemipelagic silt and clay-rich contourite deposits. (Tucholke et al., 1977) The lithologies of the sediments drilled during Leg 164 are similar to those found at prior Blake Ridge sites. The core data results show major lithology as nannofossil-rich Claystone. This consists of dark greenish gray, moderately bioturbated.

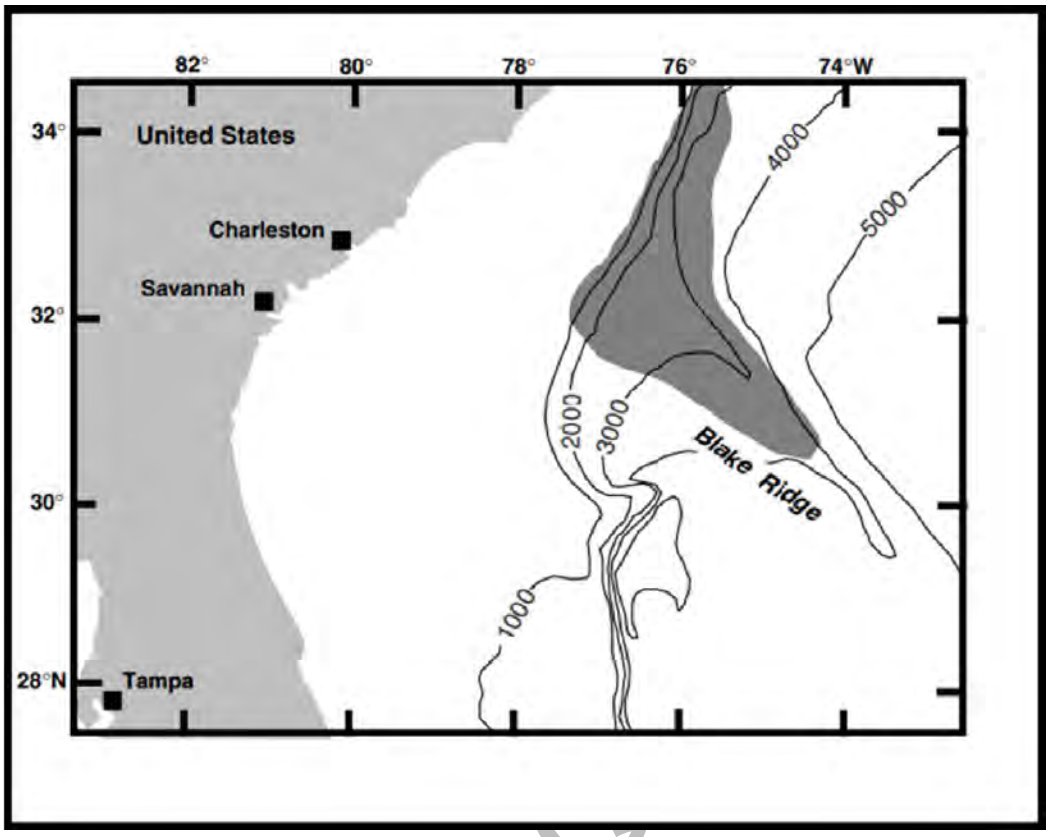

Figure 2.1: Location map showing Blake Ridge (Paull et al., 1996). Shaded area is region with seismic evidence for gas hydrate and free gas. Bathymetric contours are in meters.

Chapter 3

Seismic Interpretation and Attribute Analysis

3D Seismic data interpretation gives better understanding of accumulation of hydrocarbons in the subsurface. Usually, 3D data acquired for the development of the field from where hydrocarbons are extracted. Sometimes 3D data is used for research purpose as in this case Gas Hydrates is the research objective. This survey designed to study Gas Hydrates of Blake Ridge and understand its mechanism.

In Academics research work Well Data usually used for the synthetic seismogram to mark the seismic horizons at their positions. But in this data, there was no Well available for that purpose. Seismic attribute analysis assists in interpretation of the seismic data. Different seismic attributes gave the clear indication of Gas Hydrates.

3.1 3D Seismic Data Visualization

Three-dimensional visualization technology has now been used in the oil industry for many years. It requires powerful, expensive computer hardware that initially was not accessible to most geoscientists. Now much more powerful and cheaper PC hardware has made 3-D visualization possible for every geoscientist.

Seismic interpreters have always needed to visualize the Earth in three dimensional. The visualization of 3-D data provides vertical section and horizontal section, or time slice, side-by-side. Extensions of this idea included composite displays of one vertical and one horizontal section spliced together, chair displays and volumetric displays of various kinds.

In figure 3.1 3D cube is viewed in time and space. Line 50 is viewed in 3D in figure 3.2. Time slices at 3.8s, 4s, 4.2s and 4.4s are shown in 3D in figure 3.3.

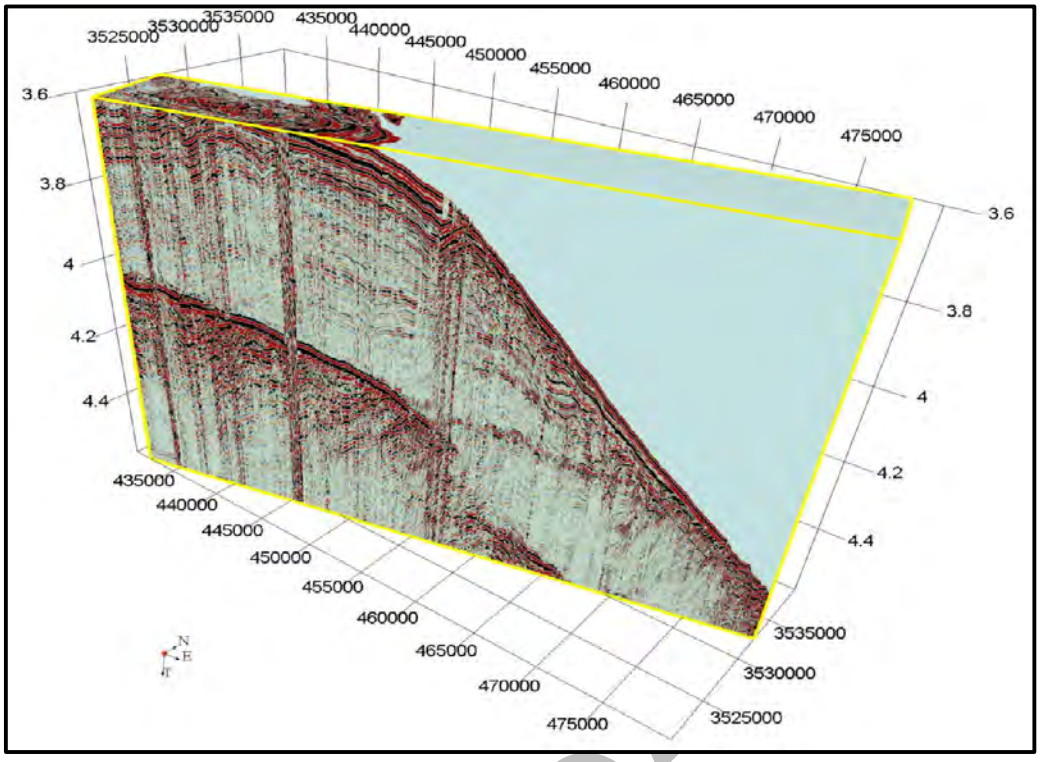

Figure 3.1 3D cube of Blake Ridge

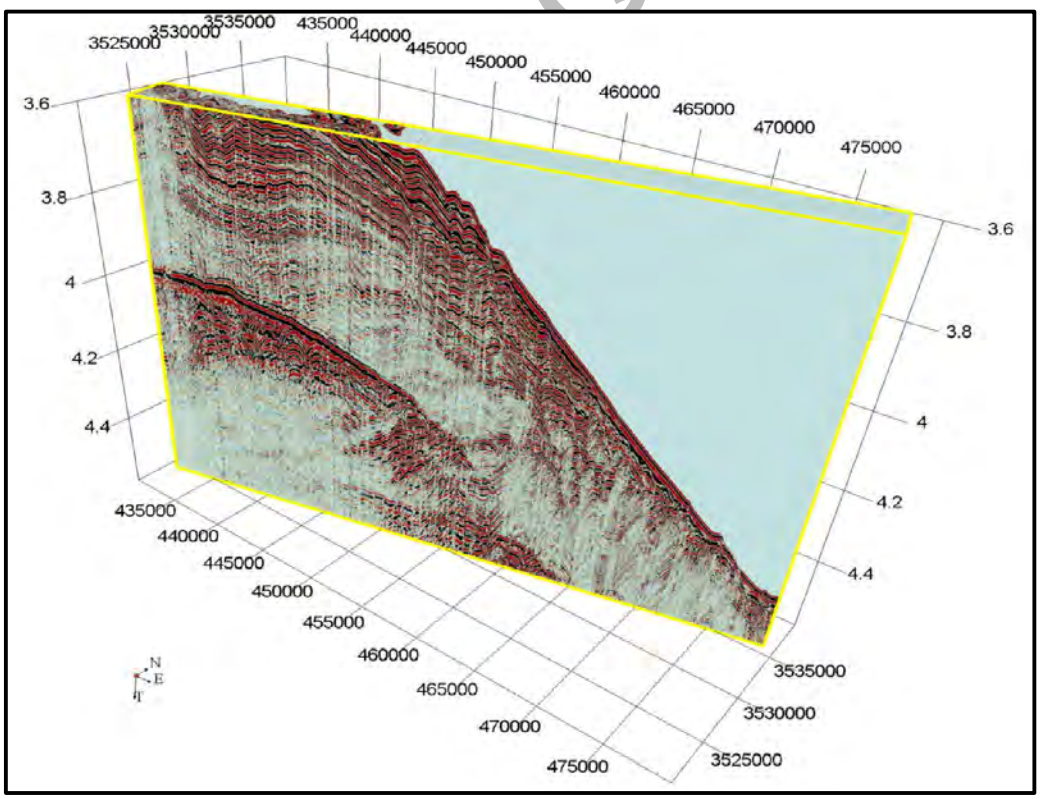

Figure 3.2 Line 50 in 3D view.

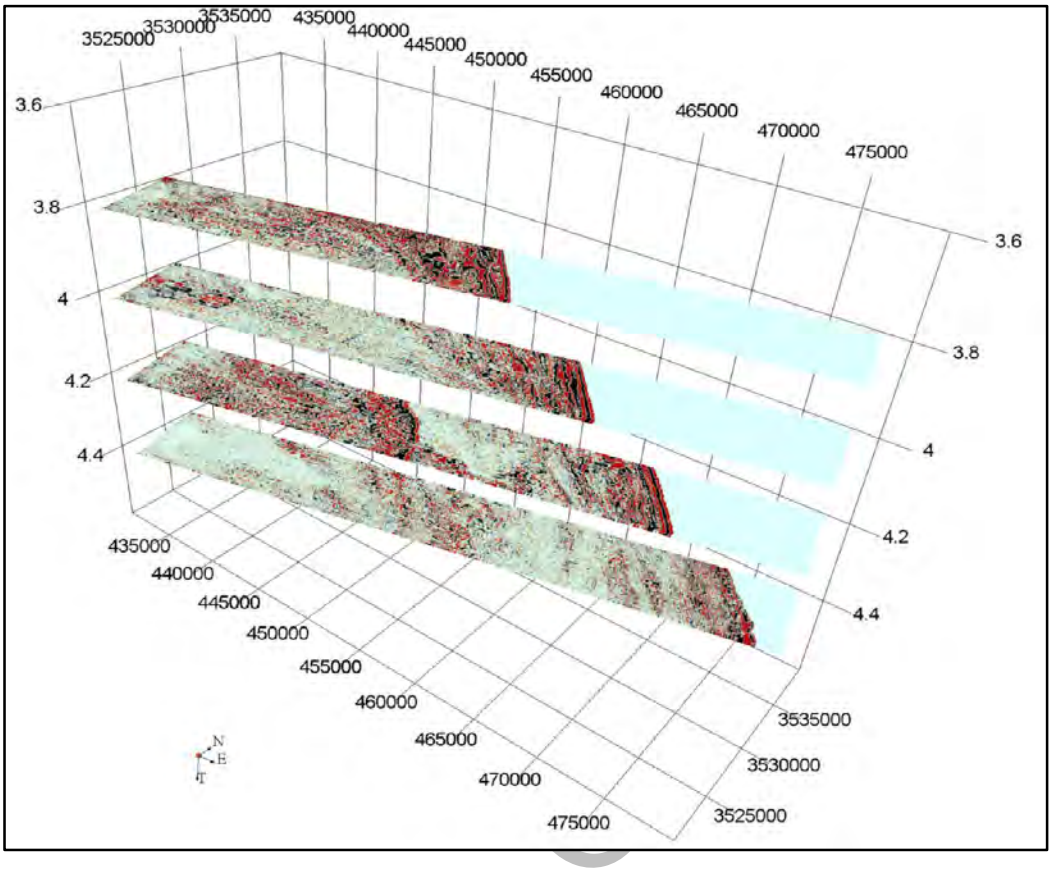

Figure 3.3 Time slices in 3D vie. Time slice at 3.8s, 4s,4.2s and 4.4s.

3.2 Gas Hydrates Reflection Characteristics

The effect of gas hydrates on seismic sediment properties is not yet understood. Solid gas hydrates have a P-wave velocity of about 3.27 km/s (Waite et al., 1998) compared to 1.5 km/s of water. It is, therefore, commonly assumed that a replacement of part of the pore water by gas hydrates increases the seismic velocity of the bulk sediment, but to what degree it depends on the microscopic distribution of gas hydrates within the sediment pores (Dvorkin and Nur, 1993; Lee et al., 1993). Gas hydrate zones are commonly underlain by a reflection that approximately parallels the seafloor, the bottom simulating reflection (BSR). BSRs are characterized by a reversed polarity compared to the seafloor reflection indicating a downward reduction of seismic impedance and hence, most likely, seismic velocity. VSPs acquired during ODP Leg 146 at the Cascadia Margin (MacKay et al., 1994) and ODP Leg 164 on the Blake Ridge (Holbrook et al., 1996) indicate that low velocities associated with free gas are the cause for the BSRs in both study areas. The free gas zone beneath the Base of Gas Hydrate Stability (BGHS) on the Blake Ridge was found to be at least 200 m

thick. It appears to coincide with a zone of high reflectivity in seismic reflection profiles. In sediments that contain gas at low concentrations, the P-wave velocity is very sensitive to gas saturation. The high reflectivity may, therefore, be explained by slight variations in gas concentration (Holbrook et al., 1996) across layer boundaries generating strong P-wave velocity contrasts and hence, strong reflection coefficients. When gas-charged strata dip relative to the BGHS, BSRs may display a shingled appearance in high resolution seismic profiles. This image is created if high reflectivity in the gas zone that is caused by slight variation of gas concentration across stratal boundaries that terminate against the BGHS. At lower frequencies, and hence larger Fresnel zones, these shingled reflections may appear as a continuous reflection. There is some confusion about the proper use of the term BSR. In this paper, we refer to it as the top of the highly reflective gas zone beneath the BGHS, even where it does not exactly parallel (simulate) the bottom. We are aware that this is a slight deviation from the original definition of the BSR. It has been suggested that a preferential accumulation of gas hydrate in higher-porosity (i.e., mostly lower-velocity) strata increases the velocity of these strata resulting in a reduction of the velocity contrast between two layers of low and high porosities. This would effectively reduce the reflection amplitude in hydrate bearing sediment sections ("amplitude blanking"; Lee et al., 1993). Holbrook et al. (1996), however, found from vertical seismic profiles (VSPs) that a uniform sedimentary section above the zone of highly reflective gas layers may be the reason for the relatively low reflectivity in the gas hydrate zone at ODP sites 994, 995, and 997 on the Blake Ridge.

3.3 Seismic attribute analysis

Seismic attributes are the set of properties computed from the data which consists of the amplitude. Attributes can be computed based on pre stacked data and post stacked data. The most common types of post stacked attributes are instantaneous attributes which are computed for every sample of the seismic trace.

3.3.1 Essential of Seismic Attributes

As our reliance on seismic data continues to grow, it is imperative that we extract as much useful information as possible from the seismic reflection data. As a result, interpreters are given the ability to glean additional information from seismic data. The extraction of geomorphologic knowledge from 3-D datasets is the focus of

seismic geomorphology, which makes use of seismic properties. When analyzing seismic reflection data, the amplitude is the property that is used by default for the determination of physical parameters such as reflection coefficients, velocities, and so on. The phase component is the most important factor that plays a role in determining the shapes and geometrical configurations of the reflectors. The actual behaviour of the complex seismic trace is explained in figure 3.4.

Attribute calculations break seismic data into constituent attributes. There is not a single rule that governs the process of computing characteristics. They can be used for determining the quality of seismic data, locating artefacts, locating petroleum prospects, evaluating hydrocarbon plays, and characterizing reservoirs. An attribute can be thought of as any quantity that can be determined from seismic data. Therefore, there are many kinds of attributes, including pre-stack, post-stack, inversion, velocity, horizon, and multi-component 4-D attributes.

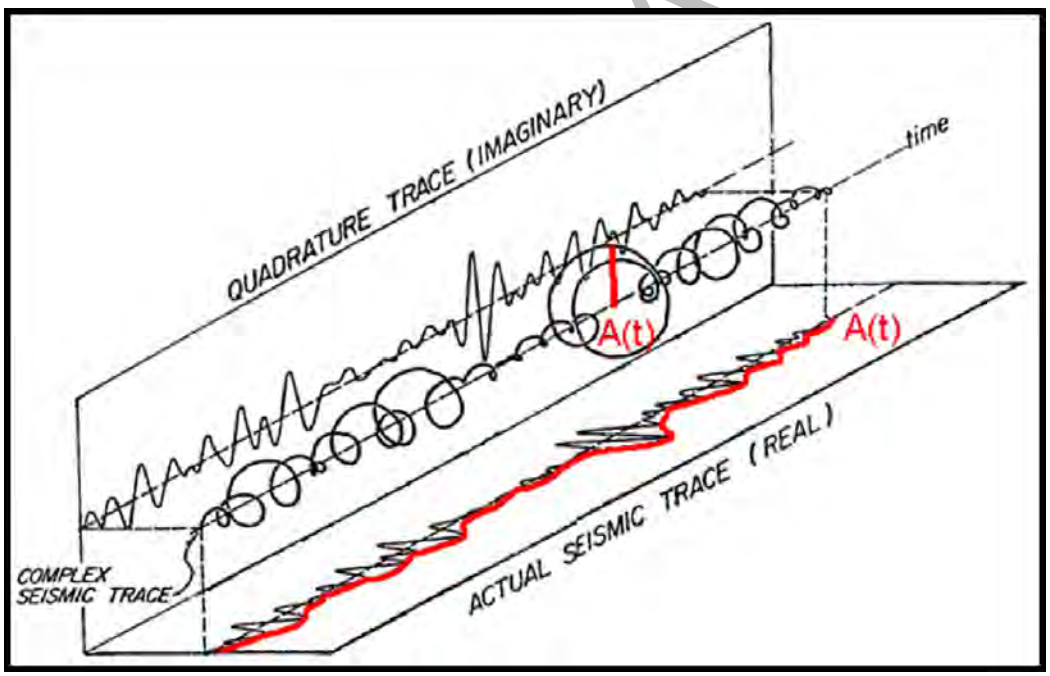

Figure 3.4 Isometric diagram for complex seismic trace showing Real (red) and Imaginary components of complex seismic trace (Taner et al, 1979)

3.3.2 Instantaneous frequency

Instantaneous Frequency (Hz) is the rate of change of phase over time(t):

$$\omega(t) = \frac{d[Phase(t)]}{d(t)}$$

Instantaneous frequencies relate the wave propagation and depositional environment; hence they are physical attributes, and they can be used as effective discriminators.

Instantaneous frequency corresponds to the average frequency/wavenumber (centroid) of the amplitude spectrum of the seismic wavelet. It indicates the edges of low impedance thin beds. Hydrocarbon indicator by low frequency/wavenumber anomaly. The unconsolidated sands, due to the oil content of the pores, sometimes accentuate this effect. Fracture zone indicator appear as low frequency/wavenumber zones. It is used for the detection of chaotic reflection zone. It can be used as bed thickness indicator. Higher frequencies indicate sharp interfaces or thin shale bedding; lower frequencies indicate sand rich bedding.

Figure 3.5 shows a plot of seismic data for inline 50 based on its instantaneous frequency. This plot shows both high and low frequencies. Under the BSR, there is a change to a lower frequency. Low frequency "shadows" imply a high level of absorption in the layers above. Gas-charged layers result in both significant absorption and a substantial decrease in P-wave velocity. So, low frequency "shadows" are usually caused by free gas if they appear under highly reflective layers that show strong velocity differences (Taner et al., 1979; Yilmaz, 1987). The change from higher to lower frequencies at the BSR is caused by free gas.

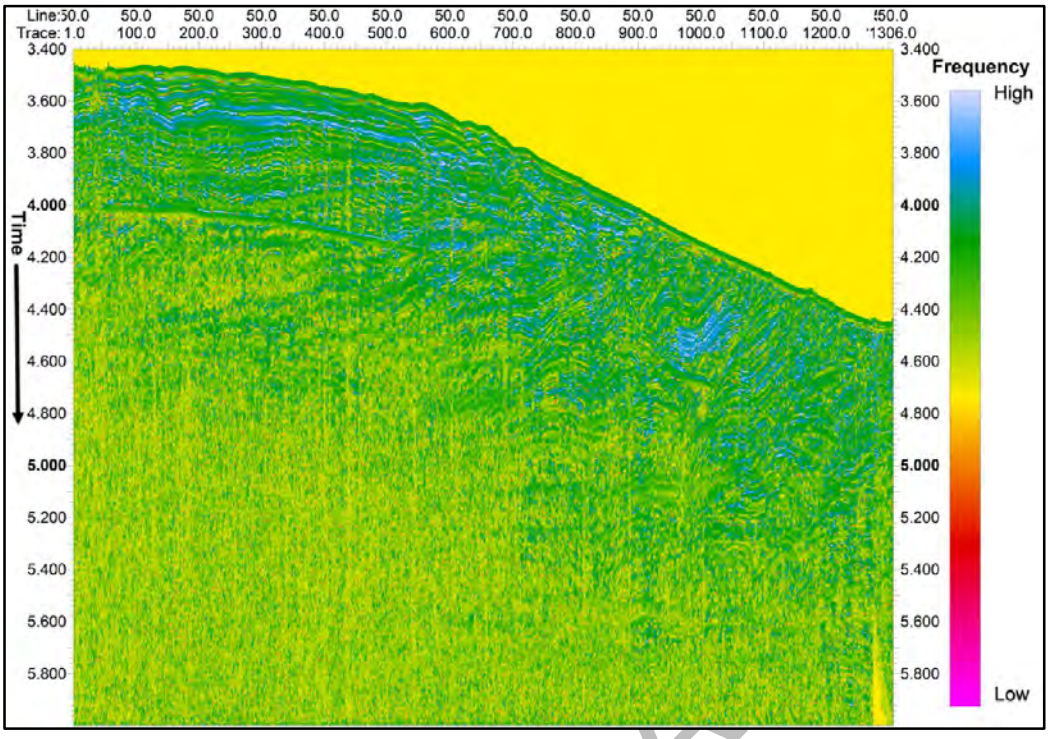

Figure 3.5 Instantaneous frequency of inline 50.

3.3.3 Instantaneous Lateral Continuity

Instantaneous Lateral Continuity corresponds to the instantaneous curvature of seismic reflections. In both inline and crossline directions, the second derivative of phase is computed. These values describe the curvature of the bed in both the inline and crossline directions. Maximum curvature is estimated in a manner comparable to that used to compute the maximum instantaneous dip. The curvature is determined on an individual sample basis.

Instantaneous Lateral Continuity attribute is used to detect linearly continuous events and it gives zero curvature value for such particular event. Beds with a hummocky appearance will have non-zero curvature values. Non-reflecting zones will have highly variable curvature values in time and space. This attribute highlights the zones of large lateral dip variation; hence it can be a good indicator of faults and fractures.

In figure 3.6 event at about 4s has linear continuity which is indicated by zero curvature value. This linear event (BSR) is formed by the presence of free gas that is base of Gas Hydrates stability zone (GHSZ). This linear event is not seen throughout

the area due limited supply of methane gas in the area. This attribute highlights the BSR and assist in interpretation of seismic data.

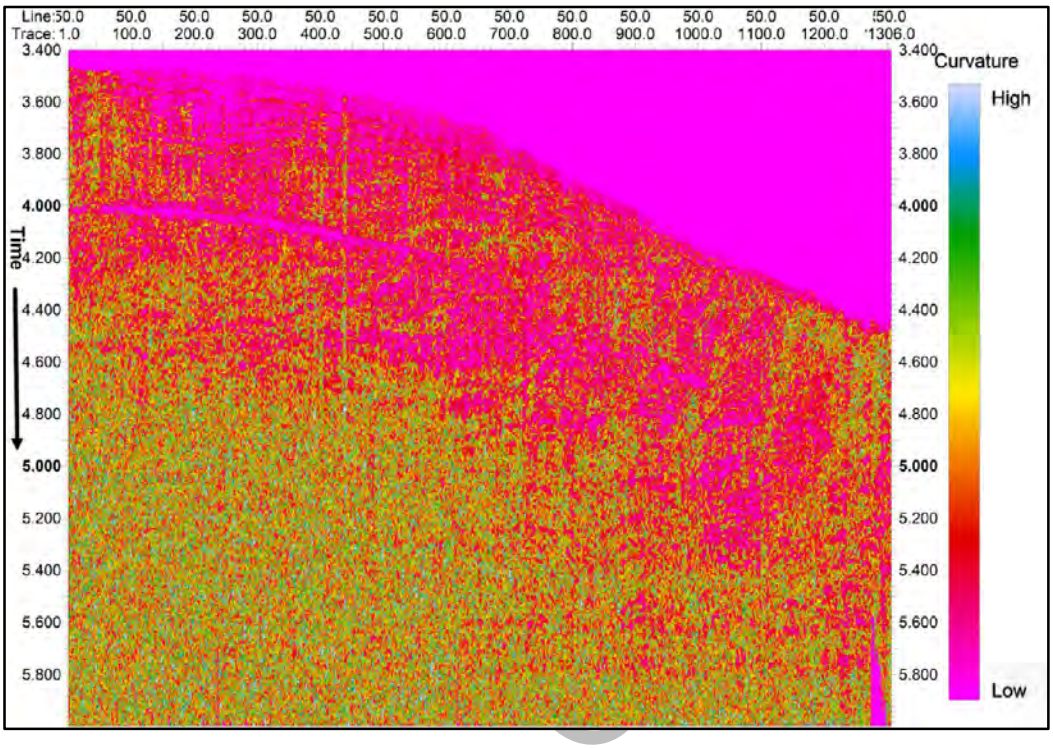

Figure 3.6 Instantaneous Lateral Continuity of inline 50.

3.3.4 Trace Envelope

Trace Envelope represents the total instantaneous energy of the complex trace independent of the phase and is computed as the modulus of the complex trace. The time scale runs from the top of the trace to the bottom. The envelope relates directly to the acoustic impedance contrast. Depending on the seismic bandwidth, it might either reflect the contrast of a single individual interface or, more often, the combined response of numerous different interfaces.

Trace envelope represents mainly the acoustic impedance contrast, hence reflectivity. It is also used to detect Bright spots and Gas accumulation. Trace envelope help to mark Sequence boundaries, unconformity, major lithology changes, or depositional environments. It also used for thin-bed tuning effects.

Trace envelope attribute indicate the change in envelope value at about 4s which implies change in acoustic impedance. This change in acoustic impedance follows the trend of Seabed which is an indication of BSR. Trace envelope also highlights the presence of Gas accumulations and that can be seen at the BSR with

high envelope values. Zone above BSR show very little or no change in envelope values and eventually acoustic impedance values which is a typical indication of Gas Hydrates marked as amplitude blanking.

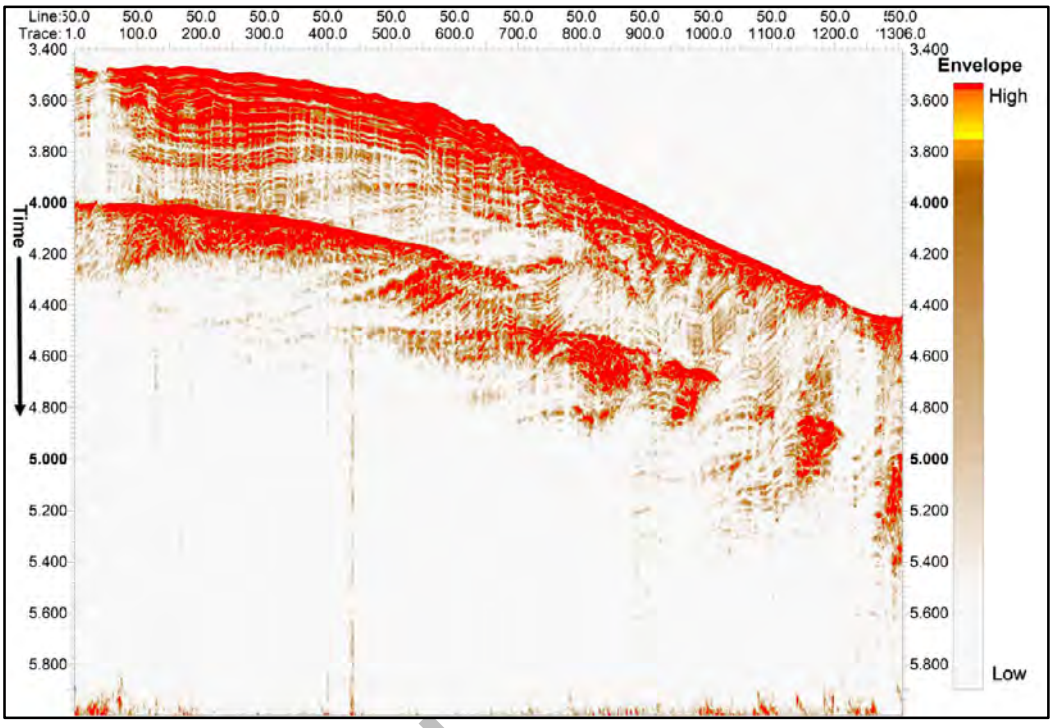

Figure 3.7 Trace Envelope of inline 50.

3.4 Seismic Interpretation

Interpretation is a technique for converting seismic data into a structural or stratigraphical model of the earth. Because the seismic section is a representation of the geological model of the subsurface, we use interpretation to attempt to pinpoint the ultimate anomalous zone. Due to the limited knowledge of real geology, it is uncommon for the accuracy or ambiguity of an interpretation to be determined. It is consistency, not accuracy, that serves as the litmus test for appropriate interpretation. A good interpretation should not only be consistent with all the seismic data, but it is also vital to know all there is to know about the location, including gravity and magnetic data, information about wells, surface geology, and geologic and physical systems. (Telford et al., 1999) Conventional seismic interpretation involves selecting and tracking seismic reflectors that are laterally consistent to map geologic formations, stratigraphy, and reservoir architecture. The objective is to identify hydrocarbon accumulations, determine their extent, and compute the quantities of these accumulations. Conventional seismic interpretation is an art that requires both a

high level of expertise and extensive practical experience in geology and geophysics. In the last three decades, there have been significant improvements made in data acquisition equipment, computer technology, and seismic processing algorithms to meet the demands of investigating ever more complicated targets. Because of this, seismic analysis has developed into a discipline that relies heavily on computing. The computer-based functioning (processing and interpretation) is more accurate, exact, efficient, and satisfying, which allows more time for further examination of the data.

3.4.1 Seismic Horizons Identification

The main task of interpretation is to identify various reflectors or horizons as interface between geological formations. This requires good structural and stratigraphic knowledge of the area (Mcquillin et al., 1984). Thus, during interpretation, the horizons are marked on the seismic section. Horizon picking is not conventional as horizon identification is done on the basis of attribute analysis discussed earlier.

3.4.2 Interpreted Seismic Section

The time section provides the position and configuration of reflectors in the time domain. Two horizons are marked on the seismic data. First is Seabed that is in blue colour. Seabed or Seafloor is the bottom of the ocean. Seabed is marked at where the first change in acoustic impedance occur below water column. Second horizon is BSR which is in yellow colour that mark the base of GHSZ or the Free Gas zone. Figure 3.8 shows the interpreted section of inline 50 with two marked horizons.

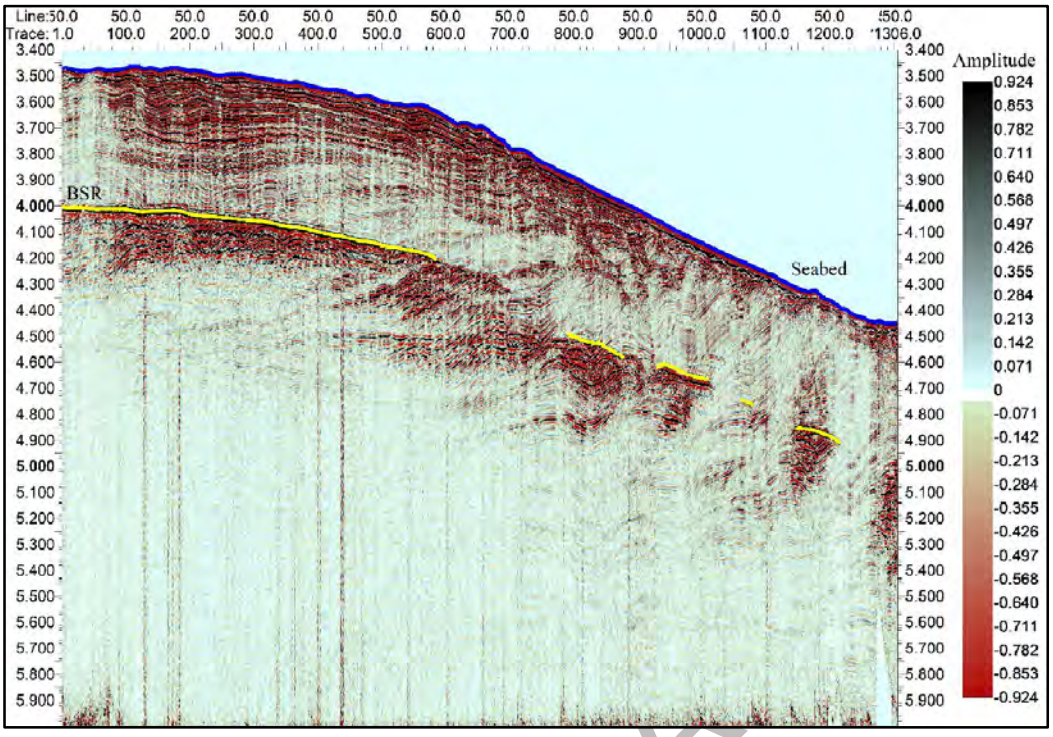

Figure 3.8 Interpreted section inline 50. Seabed (Blue) BSR (Yellow).

3.4.3 BSR Time Contour Map

The contours are equal-elevation lines (time or depth). Typically, mapping is the last result of exploration and the component on which the success of the entire operation depends (Coffeen, 1986). Using contour lines that stand for equal two-way time (TWT) below a reference datum, contour maps depict relief on horizons. These contour maps show the formation's slope, dip, and any folding or faulting that may have occurred. BSR map depicts its subsurface BSR ranges for the time of 3.998 sec to 5 sec. Map showing the increasing trend from light blue (lowest) to red (highest) value of the time.

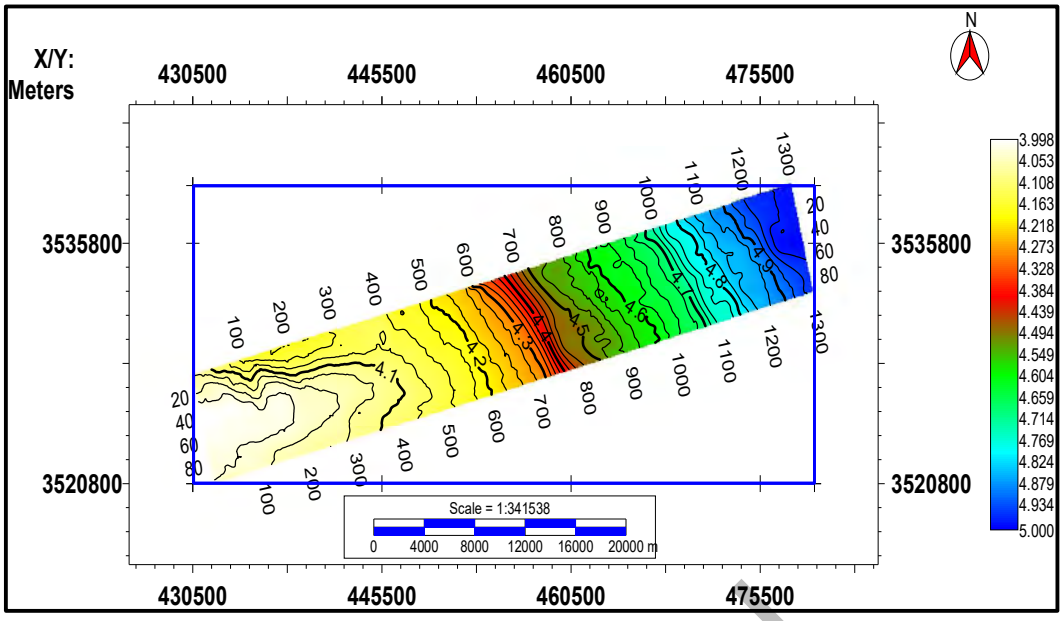

Figure 3.9 BSR time contour map

3.4.4 Seabed Time Contour Map

Time contour map gives a reliable picture of the subsurface. Seabed ranges for the time of 3.421 sec to 4.483 sec. Map showing the increasing trend from light blue (lowest) to red (highest) value of the time.

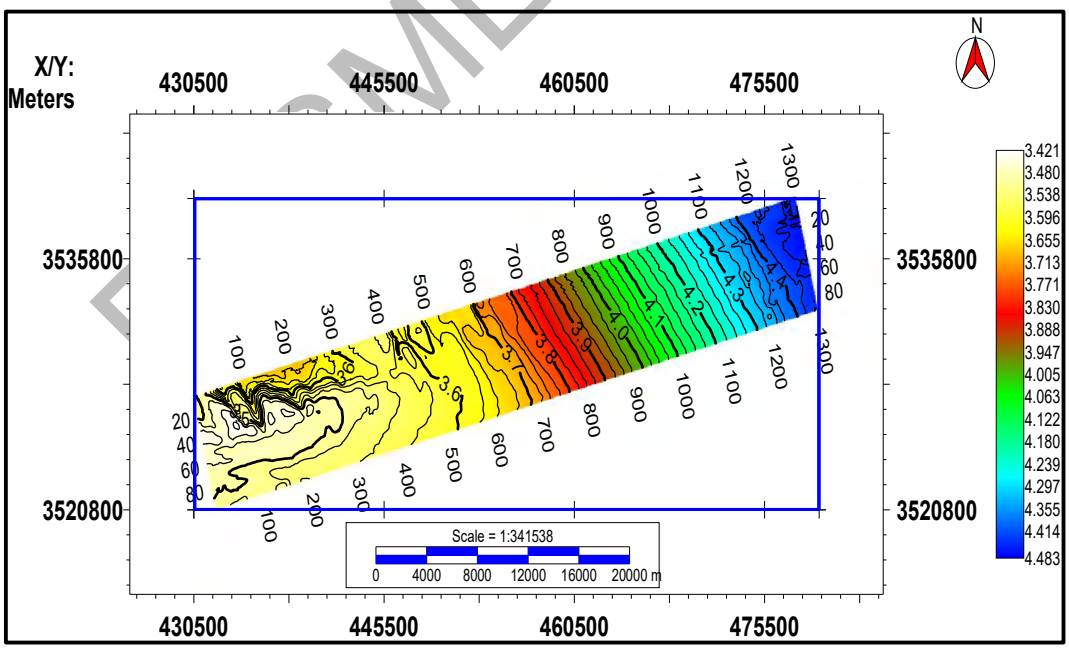

Figure 3.10 Seabed time contour map

3.5Amplitude Blanking

Previously, the substantially lower reflection amplitudes of certain sediments inside the Blake Ridge GHSZ compared to sediments below the GHSZ were interpreted as a decrease in impedance contrast and reflectivity owing to sediment cementation by gas hydrates (Lee et al., 1993). They attributed the absence of impedance contrast inside the GHSZ to the uniformity of the strata at this site, which may only be reflective underneath the GHSZ due to the existence of free gas below selectively porous layers. Holbrook et al. (1996) did not discover the abnormally high velocities that one would anticipate for frozen material. Although the velocities obtained from the VSPs reveal negligible cementation over a range of tens to hundreds of meters, the relative amplitude decrease (or blanking) may entail more than just sediment uniformity. A "blank" zone in seismic data may not always indicate a lack of impedance contrasts; rather, it may signal that there is a scarcity of nearly horizontal reflectors.

Amplitude blanking is based on the principle notion that the preferential cementation of high-porosity sedimentary layers with high-velocity hydrate reduces the impedance differences at the interfaces, which in turn reduces the amount of reflectance that is generated. This is the core concept underlying amplitude blanking. If changes in porosity are the primary source of impedance differences and hydrate preferentially grows in layers with high porosity, then the blanking hypothesis predicts that the presence of hydrate will induce decreased reflectivity in the sample (Dillon et al., 1993; Lee and Dillon, 2001). Figures show amplitude blanking quite clearly above BSR in comparison to the reflection at BSR, which may indicate the existence of hydrates.

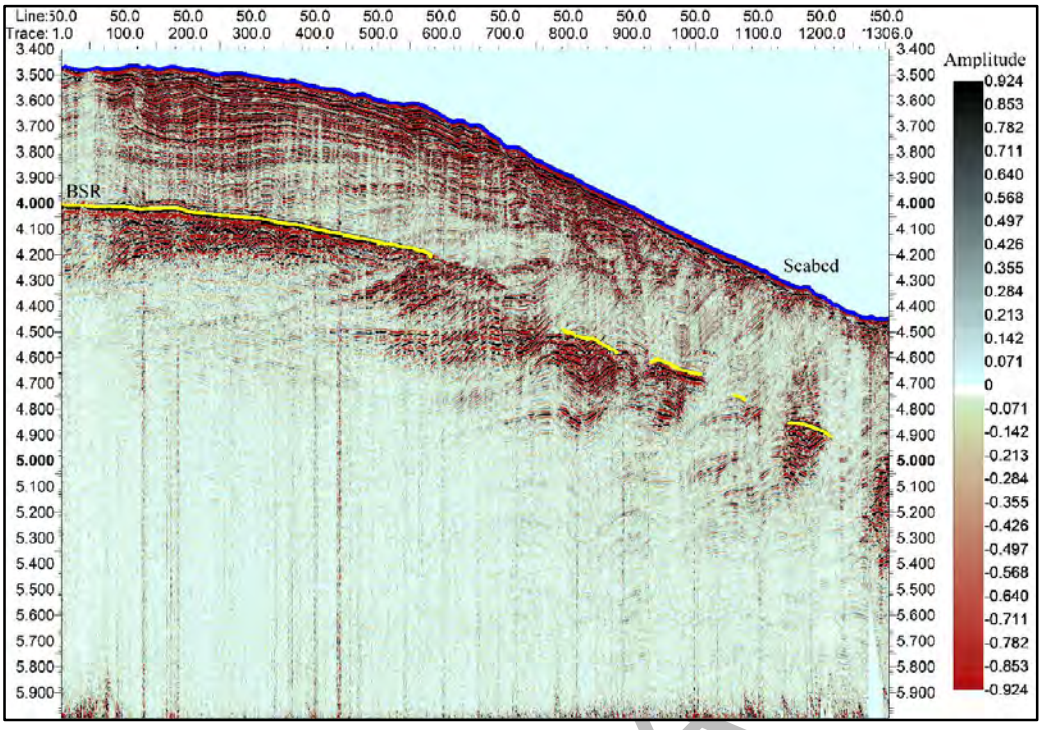

Figure 3.11 Amplitude blanking observed on inline 50.

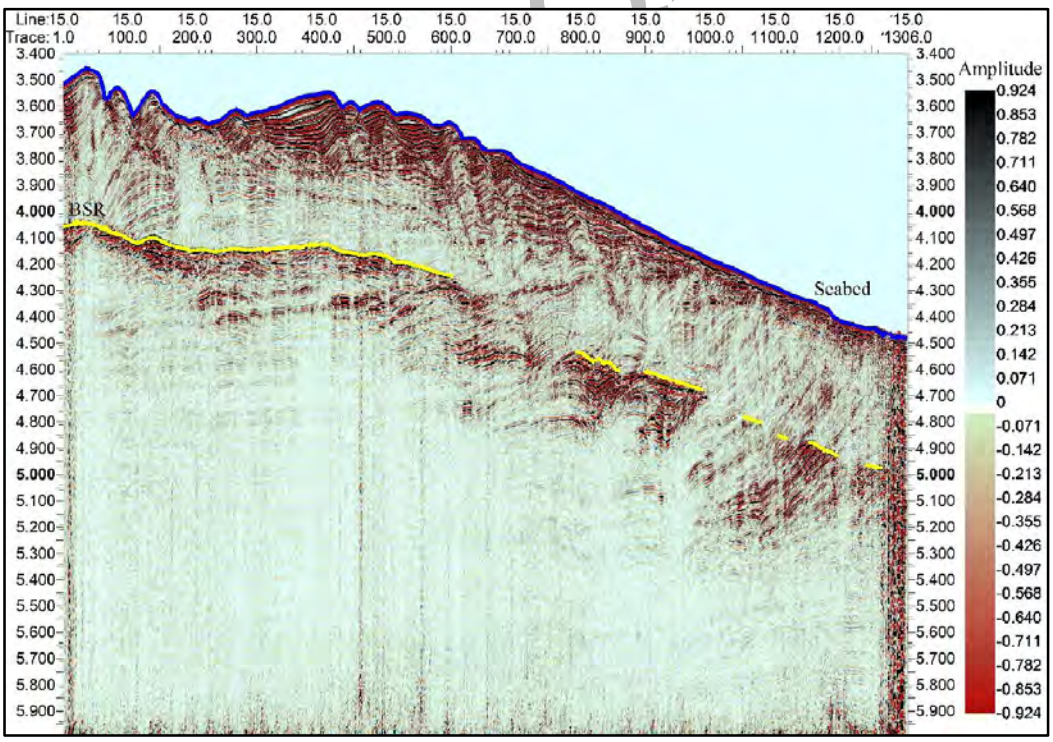

Figure 3.12 Amplitude blanking observed on inline 15.

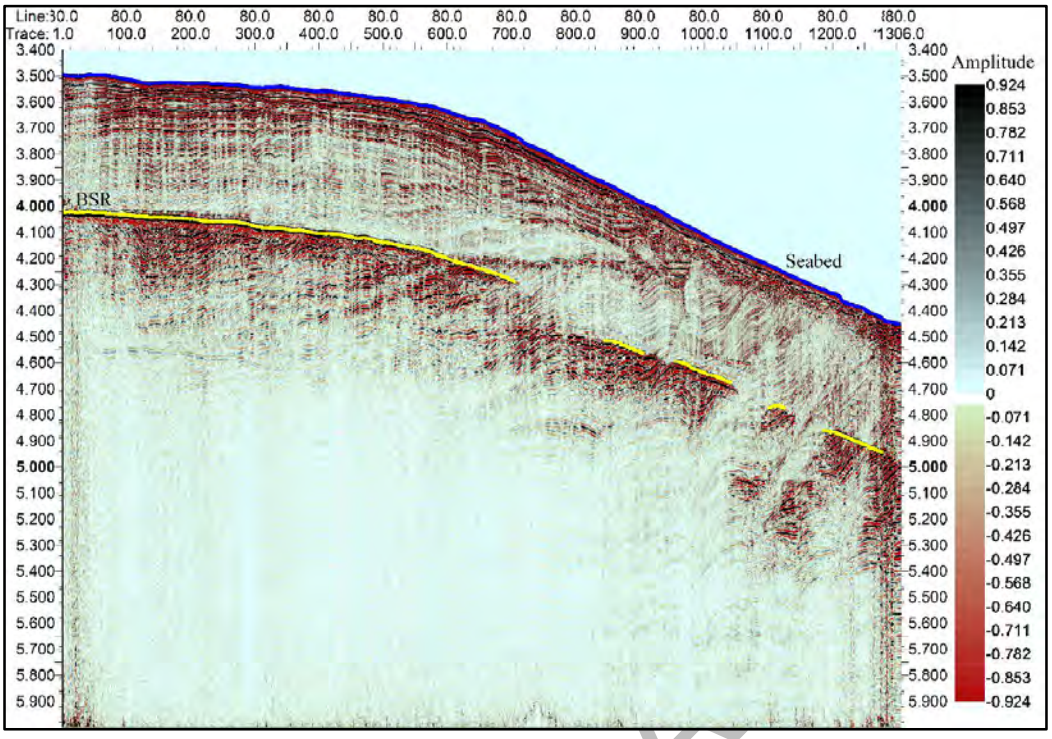

Figure 3.13 Amplitude blanking observed on inline 80.

Chapter 4

Petrophysics

Petrophysics is the analysis of the chemical and physical properties that characterize how rocks, soils, and fluids form and behave. Using well log data, core data, and seismic measurement techniques, as well as geology and geophysics, Petrophysicists analyze the attributes of the reservoir rock. Its primary use may be found in the hydrocarbon business, where it is used to investigate how various reservoirs behave. Additionally, it discusses the chemistry of the pores in the subsurface and how the pores are related to one another. It is beneficial in assisting with the regulation of the migration and buildup of hydrocarbons. Petrophysics not only explains the chemical and physical properties, but it also explains a great deal of other terminology associated with the subject, such as lithology, water saturation, density, irreducible water saturation, hydrocarbon saturation, net pay thickness, permeability, porosity, and a great deal more. The primary objective of petrophysics is to determine the characteristics of the rock by inserting various measuring devices into the bore hole.

Petrophysics incorporates the findings obtained by using a variety of geophysical instruments (such as GR, Caliper Log, SP, LLD, and LLS, among others), as well as production data and core data. The purpose of these geophysical instruments is to measure certain reservoir attributes such as porosity, shale volume, net pay, effective porosity, saturation of hydrocarbons, and so on. When it comes to reservoir description, petrophysical analysis is often less concerned with seismic data and more concerned with well log data.

The petrophysical analysis was carried out by using the wireline logs of Well 995. The log data of Well 995 is available along with necessary information of tools used and parameters while recording different logs. Gas hydrates are detected in the zone above 450 mbsf. (Lee, 2000) detected presence of gas hydrates from 193 to 450 mbsf.

4.1 Calculating Shale Volume

The source formations are composed of shale and have a higher radioactive concentration, so they have a higher Gamma Ray value. On the other side, it is also

believed that the radioactive material is lacking in other formations, which are referred to as "clean" formations since they do not include any radioactive material. This helps to highlight the differences between the shale formation and other rock types. The mathematical formulation used to calculate the Volume of Shale is given (Rider, 1986):

$$Volume\ of\ Shale\ Vshl[] = \frac{(GR[log] - GRclean)}{(GRshale - GRclean)} \quad (4.1)$$

4.2 Porosity Calculation

Porosity refers to the void area inside a rock that is not filled by particles of the rock itself. Intergranular gaps, voids caused by the dissolution of grains, and rock fractures are all factors that might contribute to the formation of porosity. The porosity of a material is denoted by the symbol "ϕ" and may be expressed either as a percentage or as a decimal. Primary porosity is produced between the grains during the time of deposition, but secondary porosity is created as a result of fracture and dissolution. The presence of secondary porosity is most often seen in limestone. In this work density is calculated using the following methods:

• Density Porosity is derived from density log using the following equation (Rider, 1986):

$$Density\ Porosity\ \phi = \frac{(Matrix\ Density - Density\ Log)}{(Matrix\ Density - Fluid\ Density)} \quad (4.2)$$

• Neutron Porosity is directly obtained from Neutron log values.

4.3 Estimation of Hydrate Amount

In this part, the fundamental aspects of the theory that are required for the calculation of the amount of hydrate that is concentrated in the pore space of the sediment are discussed. The following three-phase weighted equation may be used to represent the relationship that exists between the velocity and the concentration of hydrates in the pore. This equation forecasts the velocity of unconsolidated sediment with a high porosity, such as the sediment in the region under investigation, by assuming that the porosity remains relatively constant. The time-average equation (Timur, 1968), which estimates velocity in a hard, consolidated rock with minimal fluid, and the Wood equation (Wood, 1941), which refers to particles in suspension, are both components of the weighted equation. The weighted equation is defined as a

weighted mixture of the two equations. A three-phase weighted equation is defined as (Lee et al., 1996).

$$\frac{1}{V_p} = \frac{W\phi(1-S)^n}{V_{p1}} + \frac{1-W\phi\ (1-S^n)}{V_{p2}}, \tag{4.3}$$

where V_p = compressional (P) velocity of hydrated sediments; V_{p1} = compressional velocity of hydrated sediments computed from the three-phase Wood equation; V_{p2} = compressional velocity of hydrated sediments computed from the three-phase time-average equation; W = a weighting factor; ϕ = sediment porosity (as a fraction); S = concentration of hydrate in the pore space (as a fraction); and n = a constant simulating the rate of lithification with hydrate concentration. The three-phase Wood equation (Wood, 1941) is given by

$$\frac{1}{\rho V_{p1}^2} = \frac{\phi\,(1-S)}{\rho_w V_w^2} + \frac{\phi S}{\rho_h V_h^2} + \frac{(1-\phi\,)}{\rho_m V_m^2}, \tag{4.4}$$

where ρ_w is the density of the fluid, ρ_h is the density of pure hydrate, ρ_m is the density of matrix, and ρ is the bulk density of sediments. The bulk density is given by

$$\rho = (1-\phi)\rho_m + (1-S)\phi\rho_w + S\phi\rho_h\,, \tag{4.5}$$

The three-phase time average equation (Pearson et al., 1983; Timur, 1968) can be written as

$$\frac{1}{V_{p2}} = \frac{\phi\,(1-S)}{V_w} + \frac{\phi S}{V_h} + \frac{(1-\phi\,)}{V_m}, \tag{4.6}$$

where V_w is the compressional velocity of the fluid, V_h is the compressional velocity of pure hydrate, and V_m is the compressional velocity of the matrix. In this formulation, V_m is a modified matrix velocity as defined in Lee et al. (1996), which is the "grain" or "matrix" velocity computed at zero porosity considering the effect of clay content (Castagna et al., 1985). The amounts of hydrate concentrated in the sediment pore spaces were estimated using Equation 4.3 with parameters shown in Table 4.1.

Table 4.1. Acoustic parameters used to estimate the amount of hydrate.

	Value	Equation used	Source
W	1.1	4.3	Lee et al. (1996)
n	1	4.3	
V_w	1.5 km/s	4.4, 4.6	Lee et al. (1996)
V_h	3.3 km/s	4.4, 4.6	Sloan (1998)
V_m	4.37 km/s	4.4, 4.6	Lee et al. (1996)
ρ_w	1.0 g/ cm^3	4.4, 4.5	
ρ_h	0.9 g/ cm^3	4.4, 4.5	Sloan (1998)
ρ_m	2.7 g/ cm^3	4.4, 4.5	

4.4 Lambda-Rho and Mu-Rho

The parameters of $\lambda\rho$ and $\mu\rho$ are measures of the incompressibility and rigidity of rocks, respectively Mu-Rho and Lambda-Rho logs are calculated from the following equations (Goodway et al.,1997):

$$\lambda\rho = (\rho V_p)^2 - c(\rho V_s)^2 \quad (4.7)$$

$$\mu\rho = (\rho V_s)^2 \quad (4.8)$$

where Lambda(λ) and Mu(μ) represent the two Lame's constants. λ is a function of both compressional and shear properties of a material, whereas is purely a function of shear properties.

In Well 995 both λ and μ values are low in the zone above Bottom-simulating reflector (BSR) which supports our hypothesis of presence of Gas Hydrates.

4.5 Petrophysics Results

Above BSR different observations indicate that there may be presence of gas hydrates. There is low P-wave and S-wave velocities in the zone. P-wave velocities are low from 1550 to 1900 m/s. P-wave gently increases in the zone which indicate increasing Gas hydrate saturation towards BSR. S-wave velocities are also on lower side generally in the range of 300 to 750 m/s. Porosity in the well is high enough to accumulate the Gas hydrates in the pore spaces. Average core porosity is about 57.9 ± 3.5 % (Lee, 2000). Average density porosity is above 60%. This high porosity is the

cause that the density values are very low in the area. Density values range from 1.4 to 1.8 g/cc. Water and gas hydrates in the pores reduces the bulk density. Gas Hydrate saturation is about 6.7% in the pore spaces which is an acceptable saturation in clayey reservoirs of gas hydrates in the world.

Zone of gas hydrate can be divided into two zones, Upper and Lower zone. The upper zone of gas hydrate exists between about 2990 and 3050 m, whereas the lower zone exists between about 3150 and 3215 mas shown in figure 4.1.

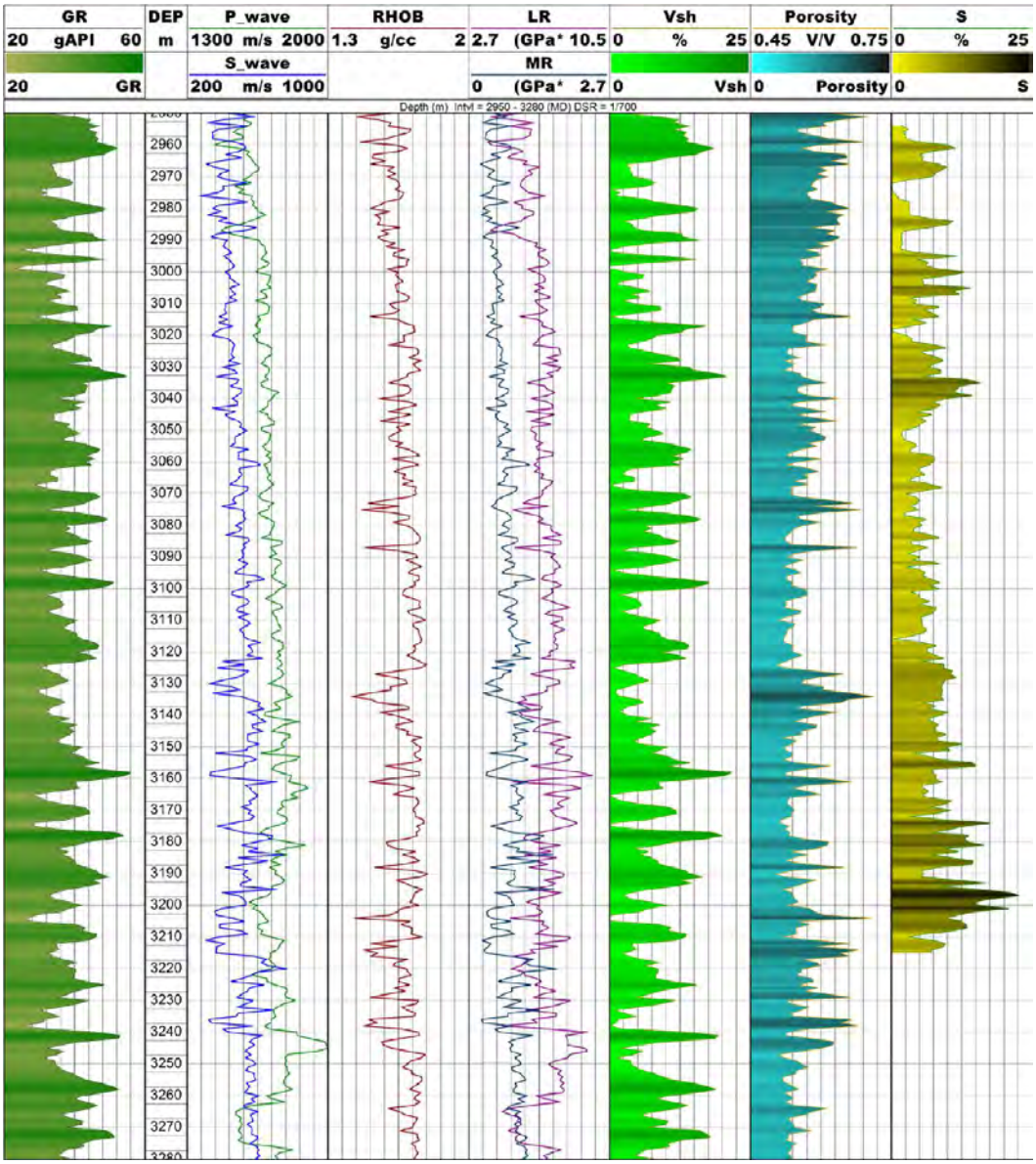

Figure 4.1 Petrophysics of Well 995.

Chapter 5

Seismic Inversion Analysis

The most effective techniques for locating possible exploration opportunities are three-dimensional seismic surveys. These seismic data volumes help identify the geometry of the reflectors and determine the depths to which they extend. Seismic waves are what make this possibility a reality. Because of the contrast in the acoustic characteristics of the material, these waves behave differently at the contact (Barclay et al., 2008). The data collected from seismic reflections includes more information than just the locations of the reflectors. The amplitude of the reflection is controlled by the impedance.

During the seismic inversion process, seismic amplitude measurements are converted into an estimate of the impedance. The amplitude of the seismic trace is a property of the interface, and the acoustic impedance is a property of the layer. It is possible to extend well information all the way up to the size of the reservoir by using a connection between seismically generated impedance and petrophysical characteristics like porosity and water saturation. Utilizing seismic inversion as a method for reservoir characterization is a key component of optimal field development.

Inversion is a technique that involves estimating, calculating, and comparing results to draw conclusions based on data that was gathered in the field. Based on the definition of inversion, a collection of mathematical procedures for reducing the amount of data to get meaningful knowledge about the physical world on the basis of conclusions derived from observations, (Sen, 2006).

In seismic inversion, porosity may be extracted, and this technique can also be used to evaluate reservoir properties. Seismic inversion, well design, and monitoring of changes in the properties of rocks because of artificial recharge or production may all be used to characterize the reservoir (Gavotti et al. 2014).

Seismic Inversion reduces the uncertainties in seismic data and is widely preferred due to its high-resolution output. The advantage of noise suppression by Initial model. Seismic Inversion determine reservoir thickness and quality and

evaluation of reservoir properties and upscaling over whole reservoir and to quantification of hydrocarbons in the reservoir.

5.1 Well-to-Seismic Tie

A well to seismic tie is required at this point because the recorded seismic data is prone to errors, and the correctness of the data may be ensured by tying it with a complete well log. Essentially, it is a quality check that is carried out as a precautionary step to limit the amount of uncertainty in the subsequent procedures. After a wavelet has been extracted, the correlation of well data to seismic data is accomplished using the approach that synthetic trace is compared with the seismic trace within the vicinity of the well. Conformity among seismic and well reflectors is achieved by slight tweaks such as squeezing and stretching of time window. Correlation coefficient and RMS error are estimated between the adjusted well synthetic and real seismic trace. This is a repetitive procedure till the results occur within a suitable range.

Well to seismic tie was done with Well 995 and inline 50. Bottom-simulating reflector (BSR) is indicated in figure 5.1. BSR position is correlated from well and seismic data to get better results in further processes.

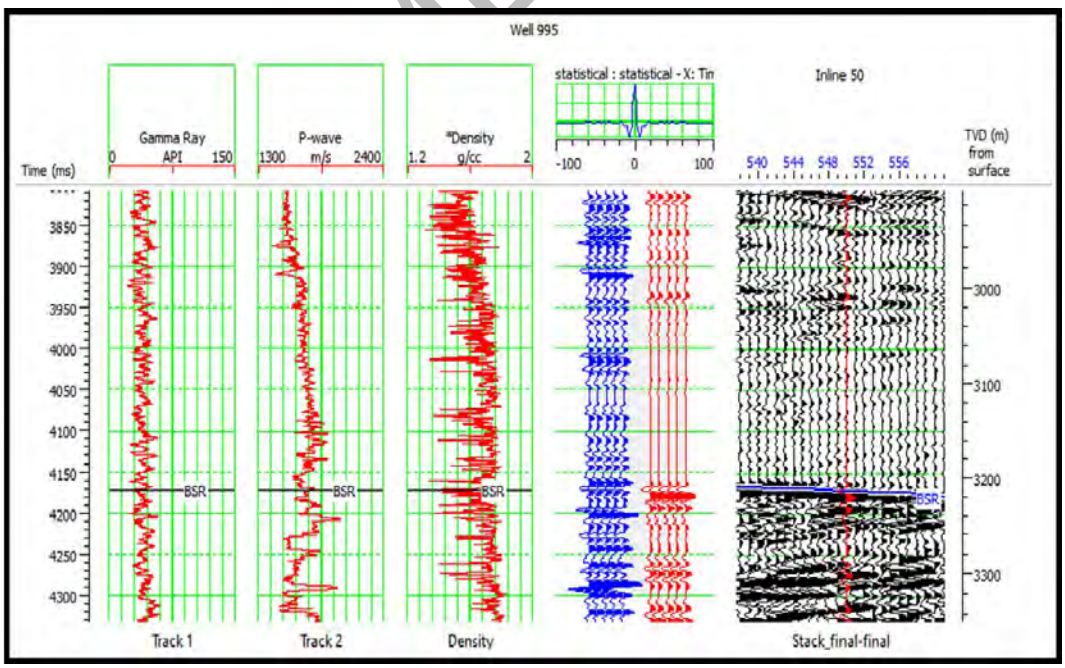

Figure 5.1 Correlation window with synthetic and real seismic trace.

5.2 Model Based Inversion

Estimating the acoustic impedance of the earth is what seismic inversion is all about. Acoustic impedance, which is a layer attribute, is used in the process of quantitatively interpreting seismic data. Impedance, which has been determined from inversion, may be used to determine the lithology, porosity, and water saturation of the reservoir zone (Kneller et al., 2013).

The generalized linear inversion method is what we work with when doing an inversion based on a model. You will be able to determine the seismic trace and wavelet, and it will attempt to adjust or change the original assumed or guessed model. This process will be performed or repeated till the synthetic trace best fits with the real or seismic trace (Gavotti et al. 2014), or, more simply, we will keep modifying the geological model until we have reduced the amount of difference that exists between the synthetic and the real seismic trace. If you have a significant amount of geological expertise, this method offers a great deal of hope to produce consistent models. (Kneller et al. 2013).

As we know, inversion is the measurement of the difference between real seismic data and simulated seismic data. Equation 5.1 shows the basic strategy of minimizing the following function, which is used in this process (Gavotti et al., 2014).

$$J = weight_1 \times (S - W * R) + weight_2 \times (M - H * R) \quad (5.1)$$

S = used for actual trace,

W = used for wavelet which is extracted

R = Final Reflectivity Series,

M = Initial supposed/guess model

H = integration operator which convolves with final reflectivity to produce final impedance.

* = convolution

In the above relation model, the 1st part is the actual trace, and the 2nd part is supposed/guess model impedance.

Modeling errors and a small amount of noise can be controlled using hard constraints (well data). Additionally, using a soft constraint (variogram model), we can incorporate an initial guess model; however, it is recommended that a hard constraint be used for the inversion procedure (Gavotti et al., 2014). The workflow for model-based inversion as shown in Figure 5.2.

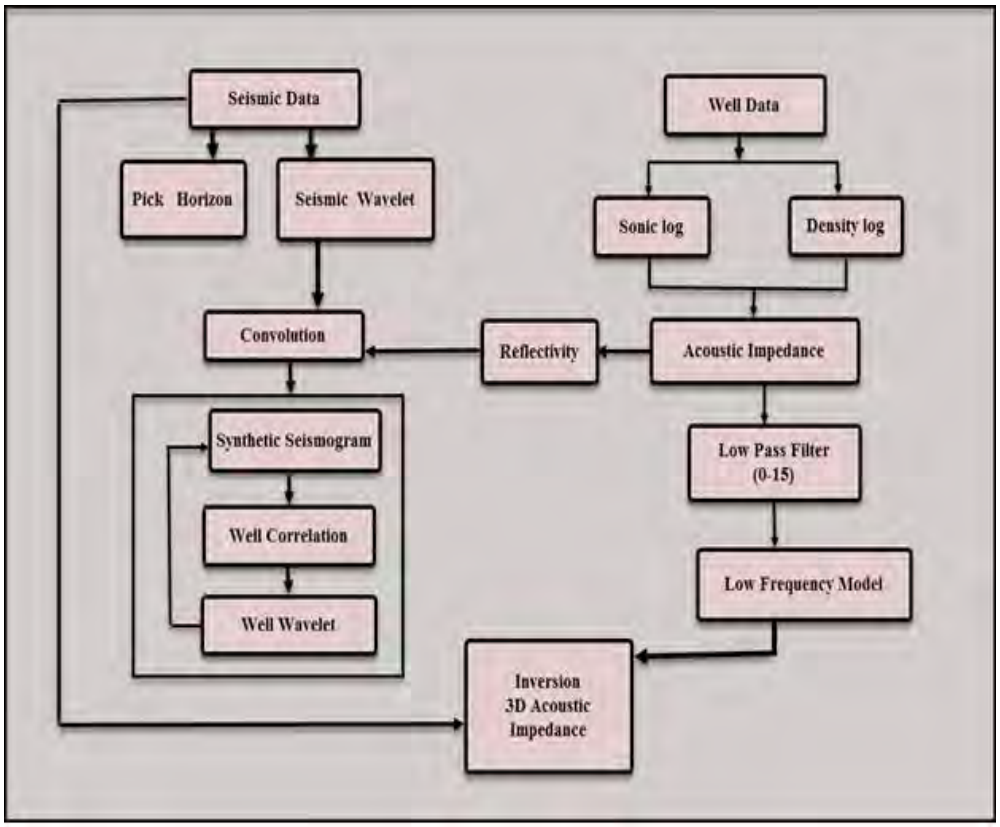

Figure 5.2 An impedance estimation scheme model on Model-based inversion. (Sen, 2006)

5.3Wavelet Extraction

The seismic wavelet creates a direct relationship between the seismic data and the geological rock characteristics, and the precision with which the wavelet is extracted has a direct impact on the outcomes of the seismic inversion. To make efficient use of inversion techniques, it is necessary to do a convolution with earth reflectivity series, which is a challenging task. Additionally, precise wavelet extraction is needed. It is necessary to put a lot of effort into the decision of which wavelet to use since, in the actual world, the shape of the source wavelet is affected by both time and depth. Geophysicists frequently favor the use of wavelets derived

from recorded seismic data over the use of any theoretical wavelet (Cooke & Cant, 2010).

Wavelet is extracted from seismic data. The wavelet is a zero-phase wavelet with frequency spectrum range from 8 to 137 Hz. Wavelet has broad frequency spectrum which helps to evaluate better evaluation of real scenario in the subsurface. Extracted wavelet is shown in figure 5.3.

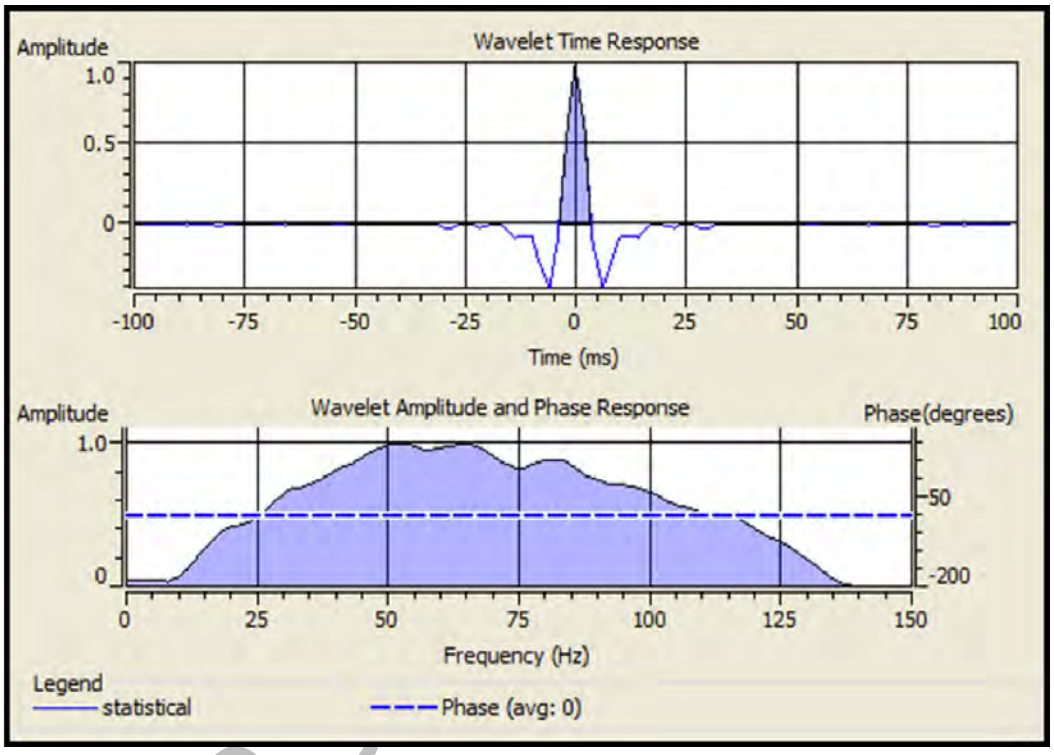

Figure 5.3 Geostatistical wavelet extracted from seismic data with its amplitude spectra. the dotted line shows the average phase of wavelet.

5.4P-Impedance Model Base Inversion

5.4.1 Initial Model/Low Frequency (LF) Model

There are two different kinds of acoustic impedance: absolute acoustic impedance and relative acoustic impedance. Low frequency models are not required for relative acoustic impedance since relative layer properties are used for qualitative interpretations. The low frequency model is required for absolute acoustic impedance because it is a layer attribute that is absolute and because it is used for both qualitative and quantitative interpretation. It converts reflectance into acoustic impedance and aids in the gathering of crucial information about formation alterations (Cooke & Cant, 2010).

The low frequency component of post-stack seismic data is often removed during the processing of the data; nevertheless, seismic inversion requires low frequencies because they include information about the background of the data (Ray & Chopra, 2016). To reclaim the frequencies that were lost during the processing of the seismic data, a low pass filter is used in the generation of the low frequency model. Low frequency model is created with the help of well data.

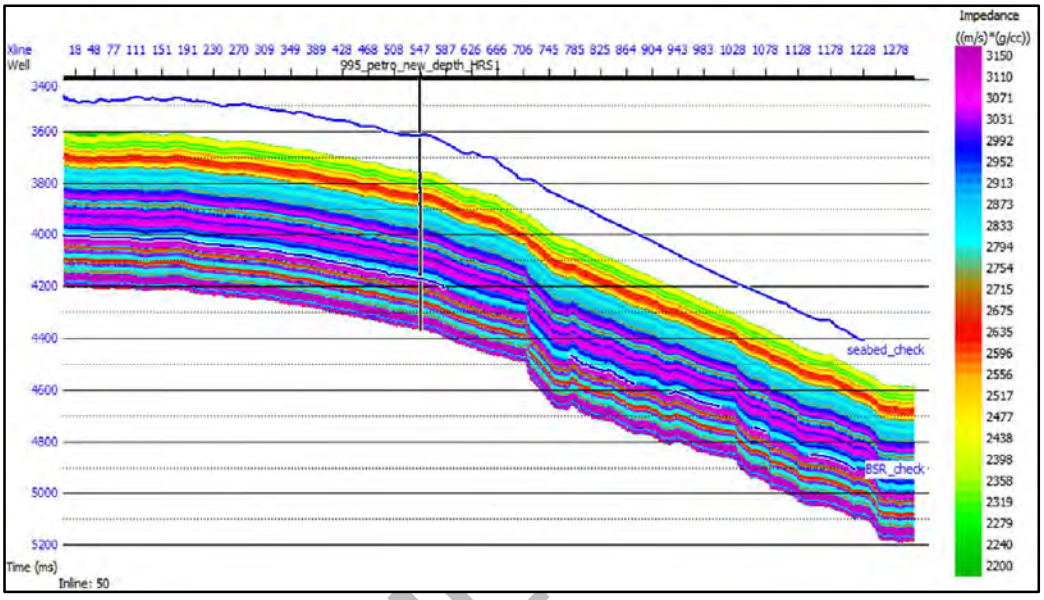

Figure 5.4 A low Frequency model showing impedance values for In-line 50

5.4.2 Inversion Analysis

At the well location the model-based inversion was performed on the given 3D seismic cube. A statistical wavelet was extracted. Frequency range of extracted wavelet was adjusted by comparing inverted trace at well location and the synthetic trace. The correlation between synthetic (red) and seismic trace (black) is good with high correlation coefficient (0.99) is shown in Figure 5.5. The estimated RMS error between the synthetic and seismic trace is 0.05 The estimated RMS error between the inverted trace and the impedance log was 139.39 (m/s) *(g/cc).

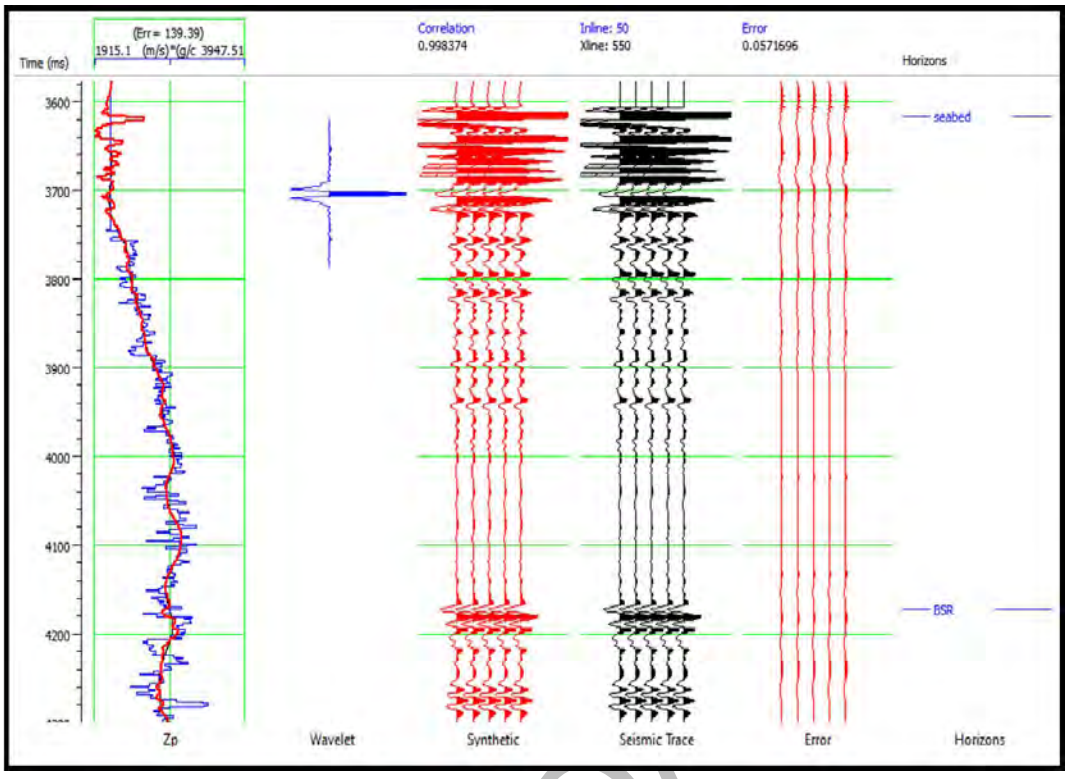

Figure 5.5 Best fit correlation model of synthetic and real seismic trace

5.4.3 Inverted P-Impedance Section

Result of model base inversion is inverted volume. This impedance is then used for the estimation of reservoir parameters on seismic scale. Inverted P-impedance section of inline 50 is shown in figure 5.6. The curve show P-impedance curve, which demonstrate high impedance zone above BSR which is an indication of presence of gas hydrates. High values of impedance which are an indication of gas hydrates as hydrates P-wave velocity is high than water.

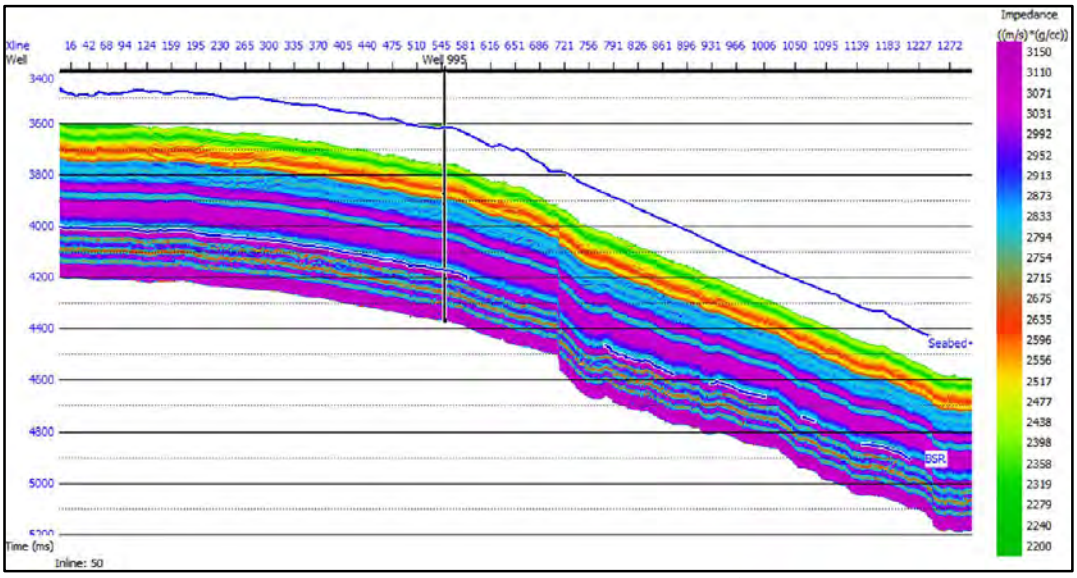

Figure 5.6 Inverted P-impedance section for inline 50

5.5 S-Impedance Model Base Inversion

5.5.1 Initial Model/Low Frequency (LF) Model

The low frequency model is a highly significant and potentially fruitful avenue for getting absolute rock characteristics. There is evidence of a low frequency spectrum in the post stack data. Because they originate from ground roll, low frequencies are eliminated during the processing stage. However, they are an essential part of the seismic inversion process. In the process of delineating thin beds, low frequency is of utmost significance. In the absence of low frequency, a tuning effect is formed, and this is the cause of the inability to resolve thin beds. The narrow bed problem could be solved by incorporating low frequency into the original model. (Al-Rahim et al., 2016).

When we include low frequencies in our model, the acoustic impedance may be easily calculated. The issue of non-uniqueness is still present in inversion, even though the addition of input data from sonic and density logs has made the results derived from low frequency far more dependable.

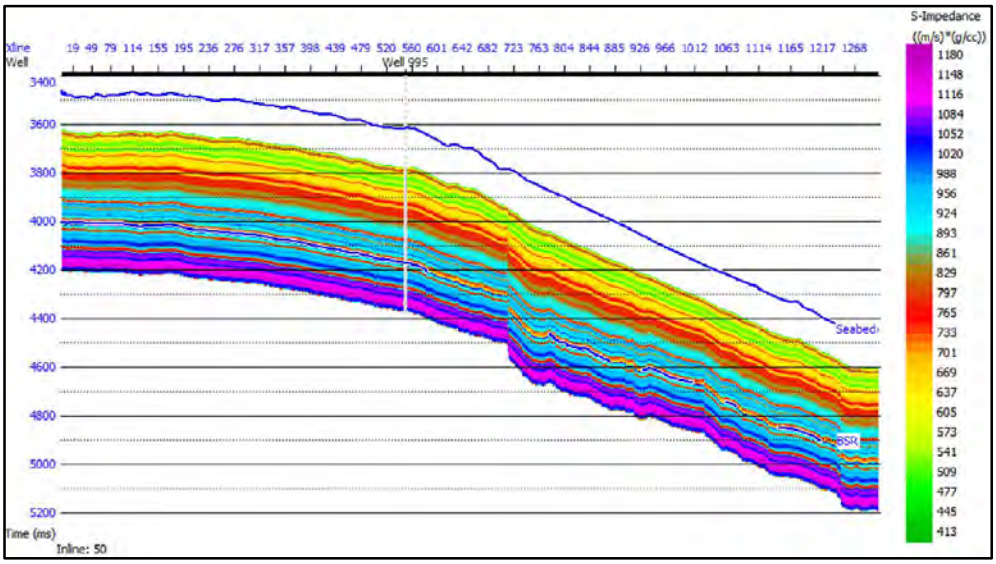

Figure 5.7 Initial Low Frequency Model generated by using the S-impedance curve

5.5.2 Inversion Analysis

The correlation between synthetic (red) and seismic trace (black) is good with high correlation coefficient (0.98) is shown in Figure 5.4. The estimated RMS error between the synthetic and seismic trace is 0.19 The estimated RMS error between the inverted trace and the impedance log was 83.93 (m/s) *(g/cc).

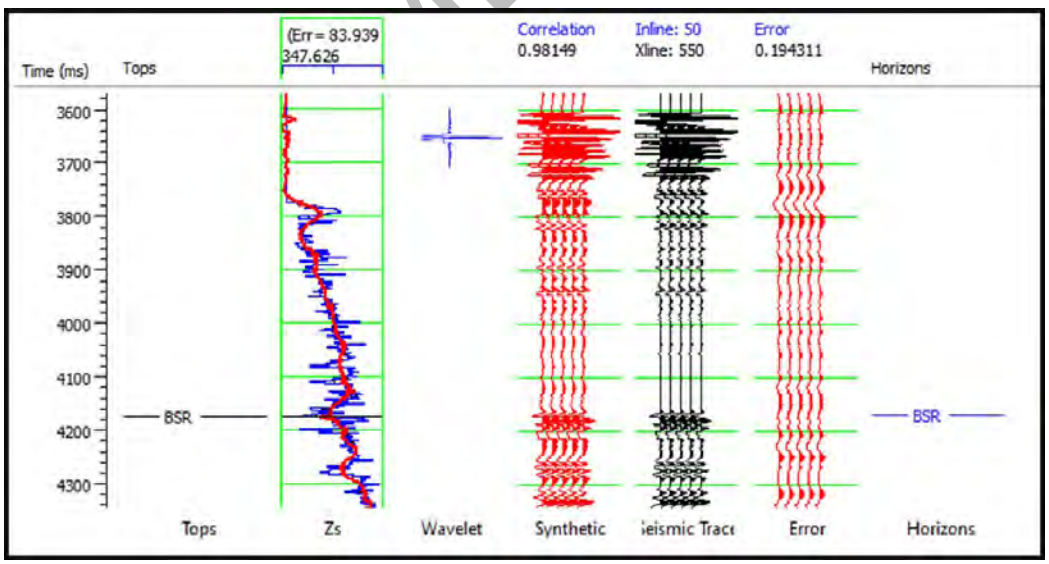

Figure 5.8 synthetic trace from inversion (red) and extracted trace from the seismic (black)

5.5.3 Inverted S-Impedance Section

Above BSR S-impedance section supports the presence of hydrates with high S-impedance values.

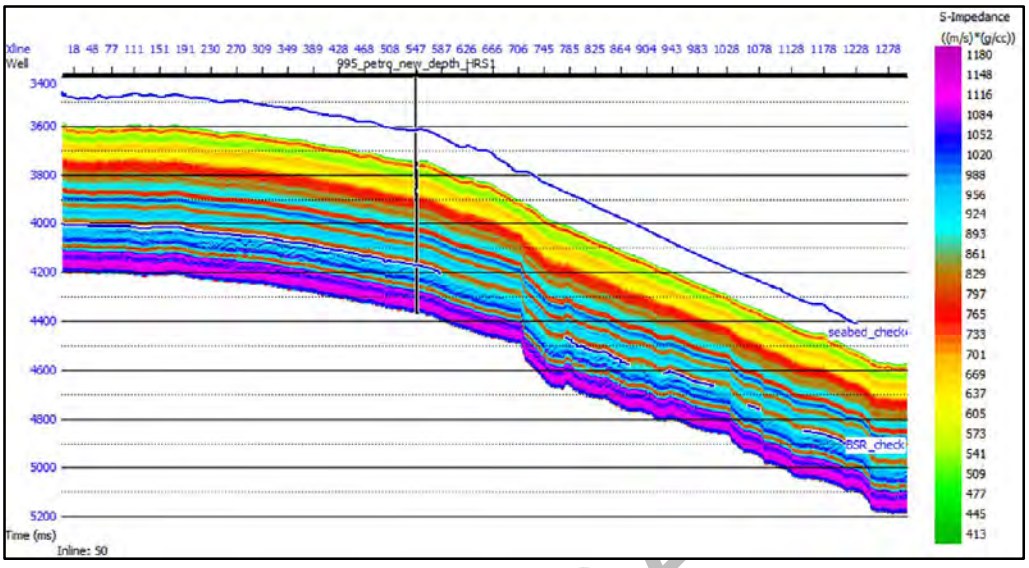

Figure 5.9 Inverted S-impedance section for inline 50

Chapter 6

Estimation of Parameters

6.1 Lambda-Mu-Rho (LMR) Inversion

Using the rock physics analysis and inversion workflows together is a more reliable method. This is done by converting the model-based inversion output volume into Lambda-rho and Mu-rho. In this model, the Lambda and Mu parameters were added using Lame's parameter (λ and μ), and density and the LMR model are fundamental elements of the new simultaneous inversion technique. The relationship between lambda and rho may be seen in Equation 6.1 (Goodway et al.,1997).

$$\lambda\rho = (\rho V_p)^2 - c(\rho V_s)^2 \quad (6.1)$$

where V_p, V_s, and ρ represent the P-wave velocity, S-wave velocity, and density, respectively, and c represents a constant that has a value of 2. Russell et al. (2003) hypothesized that if the well log data is available, then c for a particular configuration of a basin may be computed locally. The constant c, which varies depending on the geological setting, has an impact on the outcome of the fluid calculation. The value of c is within the range that was established by Dillon et al. (2003), which is relevant for both offshore and onshore environments. The value of Mu-rho is equal to the square of the S-wave impedance, which represents rigidity (rock matrix) and is provided by equation 6.2 (Goodway et al.,1997).

$$\mu\rho = (\rho V_s)^2 \quad (6.2)$$

The LMR inversion is a powerful technique that can help in characterizing lithology. Figure 6.1 displays the profile image of the lambda-rho attribute applied on the inline 50 of well 995 where the lambda-rho property shows values, with the maximum range having a purple color and value of 8.51 (GPa*g/cc), and a minimum represented by green color and a value of 3.58(GPa*g/cc). The Mu-rho property is sensitive to the rock matrix with a maximum to minimum range of 1.25 to -0.02 (GPa*g/cc) in figure 6.2, color varying from green (minimum) to purple (maximum). Overall lambda-rho and mu-rho values in the area on the lower side which the strata is compressible as well as less rigid. These results support the presence of gas hydrates.

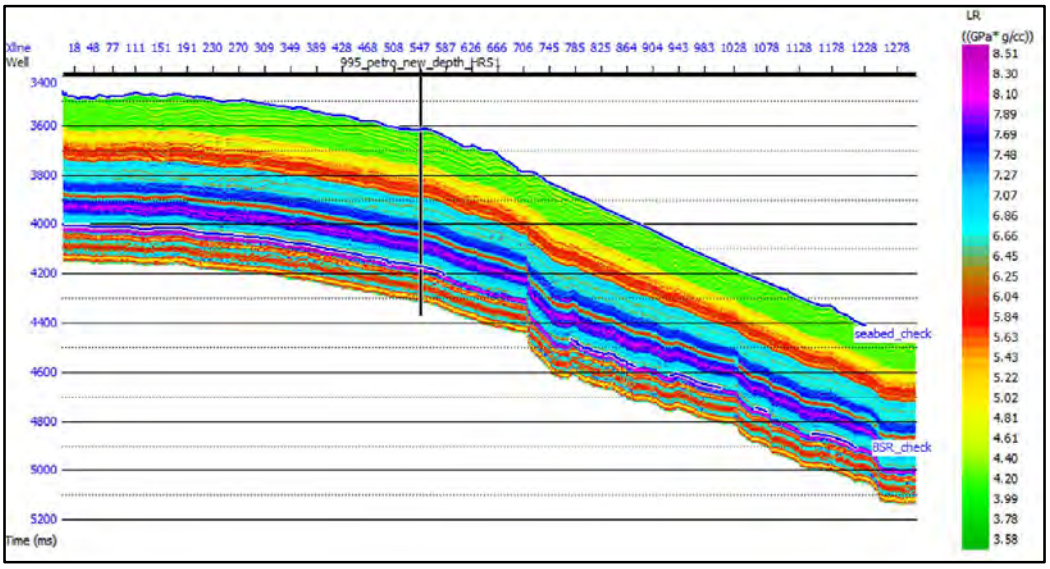

Figure 6.1 Lambda-Rho section of inline 50.

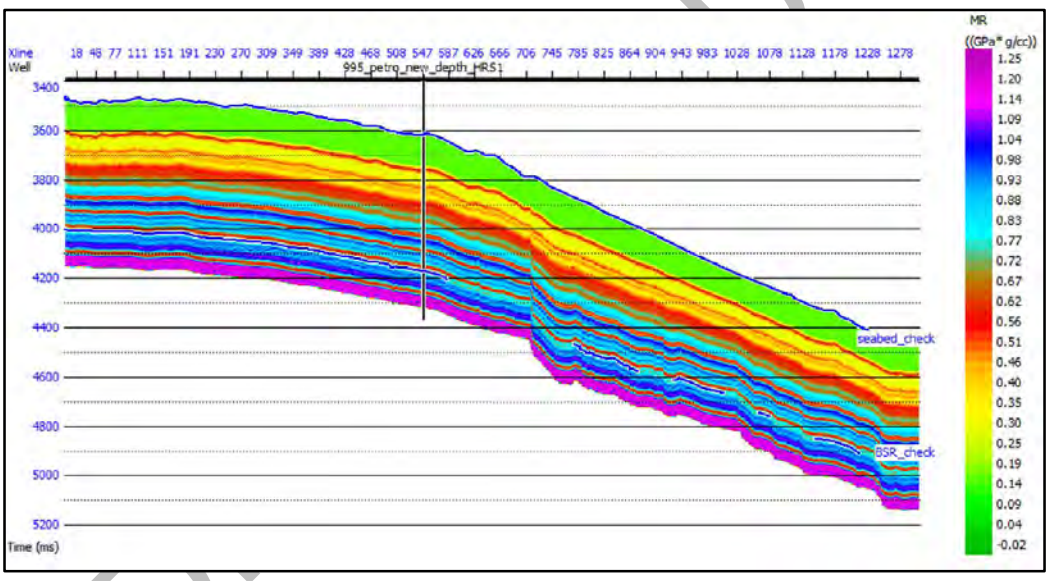

Figure 6.2 Mu-Rho section of inline 50.

6.2 Porosity Estimation

In seismic post-stack inversion, the primary objective is to get the porosity distribution throughout the whole of the seismic data in order to characterize a reservoir in a region. Cross-plotting allows one to determine that there is a linear and inverse connection between p-impedance and porosity. The regression line is drawn across the data points with acceptable correlations greater than 83%. Figure 6.3 depicts a cross-plot between p-impedance and porosity.

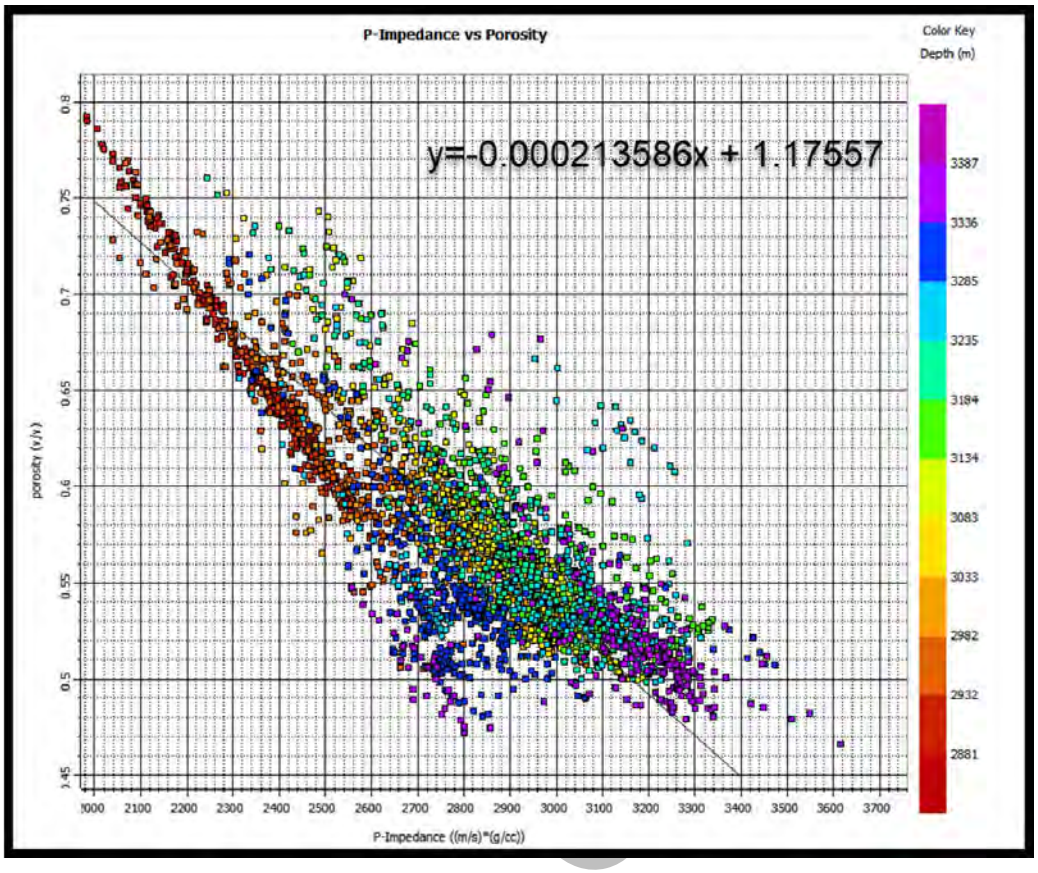

Figure 6.3 Cross plot of porosity and P-Impedance

Porosity section computed with the relation obtained from cross plotting porosity and P-impedance. The equation is as:

$$y = 0.000213586x + 1.17557 \qquad (6.3)$$

Porosity section is generated from the inverted P-impedance obtained from model base inversion as shown in figure 6.4. Equation 6.3 used to generate porosity section which shows high porosity across the area. High porosity can accumulate hydrate concentration in addition to water.

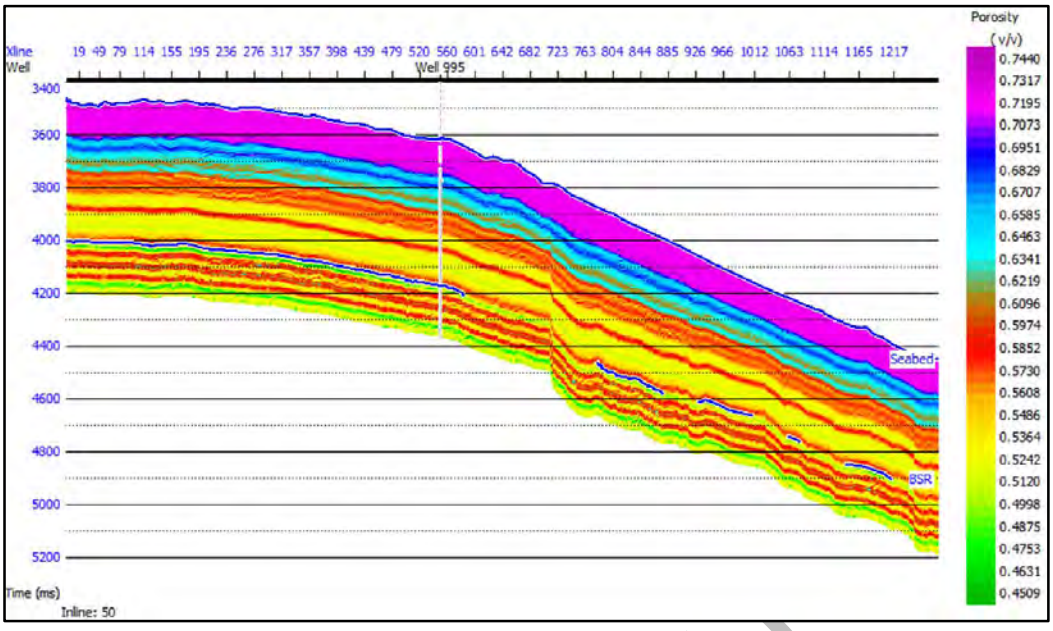

Figure 6.4 Porosity section of inline 50.

6.3 Hydrate Saturation Estimation

Hydrate saturation on the seismic scale is determined from Probabilistic Neural Network (PNN). PNN is one of the most attractive algorithms because of its capacity to build non-linear connections between the input and the target attribute. This ability makes PNN one of the most intriguing algorithms. It learns the relationship between the target log and the seismic parameters at well sites by analyzing the seismic data. After that, it makes use of the information to make a prediction on the desired property in a seismic segment. According to Tonn (2002), PNN is dependent on a method of mathematical interpolation that is realized via the NN design. This is a possible benefit since it allows us to comprehend the behavior of its theoretical analysis much better than the multilayer feed-forward neural network (MLFN). Its relative ease of mathematical understanding makes it seem to be the network of preference (Hampson et al., 2001). The PNN offers several benefits over the MLFN in addition to these. To begin, it is not dependent on a primary group of weights when it is first applied. Second, since the weights are wholly determined by the data, there is no difficulty with the way in which they converge to a solution (Herrera et al., 2006). The PNN has a number of drawbacks, the most notable of which are that it is possible for it to be slower than the MLFN and that it requires more memory in order to store the mod. The purpose of the PNN is to locate weights that are dependent on the distance that separates the input point from each of the

training points. This distance is calculated in a multidimensional attribute space and scaled using smoothers produced by cross validation. After that, the unknown log values are figured out by multiplying the weighting functions by the known log values (Hampson et al., 2001). During the training phase of the network, PNN makes use of Gaussian weighting functions to ensure that the seismic properties (x) are appropriately matched to the samples (x_i). Each training sample is centred on the Gaussian normal distribution, and the method determines the smoothing value (σ_j). According to Todorov (2000), the PNN is characterized by the following basic equation:

$$y'(x) = \frac{\sum_{i=1}^{n} y_i \exp(-D(x,x_i))}{\sum_{i=1}^{n} \exp(-D(x,x_i))} \qquad (6.4)$$

Where y' = the new log value, n = total number of training samples, y_i = the measured target log values, and $D(x, x_i)$ = the distance between the input seismic attribute (x) and each of the training points (x_i) and is given by

$$D(x, x_i) = \sum_{j=1}^{p} \left(\frac{x_i - x_{ij}}{\sigma_j}\right)^2 \qquad (6.5)$$

where σ_j = smoothing parameter, and p = the number of seismic attributes. Cross validation is utilized to determine the ideal set of smoothing parameters by excluding a portion of the training data (Hampson et al., 2001). The conjugate gradient method is then implemented to reduce validation errors (Todorov, 2000; Mohamed et al., 2019).

PNN involves the derivation of seismic attributes. Seismic attributes are measured, and characteristics estimated from seismic data, including the time, amplitude, frequency, and attenuation of seismic waves (Eichkitz et al., 2013; Sarhan and Safa, 2017). Physical and geometric characteristics classify seismic features. The physical characteristics are closely related to lithology and other physical parameters; they are classified as pre-stack and post-stack attributes, with instantaneous and wavelet subclasses for each. The geometric properties are the fundamental information gained from seismic observations, including time, amplitude, frequency, and attenuation, and are classified as dip variance, azimuth, and discontinuity (Subrahmanyam and Rao, 2008; Eichkitz et al., 2013). In comparison to a few years ago, there is little doubt that the output quality of seismic attributes has vastly

improved. Additionally, it can be used to predict logs between well locations. The application of characteristics facilitates the investigation of a number of essential rock physics parameters and their distribution along a reservoir (Halleland et al., 2007; Othman et al., 2018; Ismail et al., 2020b). So, several types of post-stack attributes are helpful for imaging gas chimneys and channels (Ismail et al., 2020c; Monier et al., 2021) and other types of conventional and unconventional hydrocarbon reservoir rocks in different basins in any part of the world with similar geological settings. Geometrical, stratigraphic, and hybrid seismic attributes are modern and well-known geophysical technologies for the detection of deep seafloor pockmarks and gas pipelines, as well as for revealing information on geological formations in minute detail (Ismail et al., 2021). These are the steps involved in the PNN workflow. The first phase involves loading seismic and well-log data and driving internal attributes. The seismic data includes the entire stack seismic section and the P-impedance obtained through inversion, which were respectively loaded as internal and exterior attributes. The hydrate saturation log for the well was loaded as a target log to ensure that the post-stack seismic inversion data matched the well-log data. A multi-attribute analysis employs stepwise regression, which determines subsets of characteristics based on internal and external attributes. According to Herrera et al. (2006), distinct types of characteristics include instantaneous attributes, integrated attributes, time, windowed frequency attributes, filter slices, and derivative attributes. Using nonlinear transformations such as natural log, square root, square, exponential, and inverse, these characteristics can be enhanced even further (Mohamed et al., 2017). Due to the disparities in frequency content between the log and seismic data, sample-by-sample correlations between the log and the characteristics may not have been satisfactory. To connect each sample of the target log to a group of neighboring samples on the seismic attribute, a convolutional operator was used (Hampson et al., 2001). When the mean-squared error in prediction is lowered, the convolutional operator is extremely effective (Mohamed et al., 2017). Cross-validation is used to discover which seismic features are the best after evaluating all of them and retaining the ones with the lowest prediction error. Far from the training wells, the convolutional multilinear regression coefficients are applied to seismic traces. The result is a seismic section of reservoir parameters. Multilinear relationships are improved using nonlinear relationships such as PNN. The multi-linear regression ranking and number of characteristics are given to a NN algorithm for extra training in the second stage. Using this nonlinear

connection, the well log property can then be determined at every site along the seismic section. In cross-validation, wells are excluded from the training phase and predictions are made blindly. Before employing the NN, this method establishes a degree of trust in its precision (Herrera et al., 2006). Using the trained NN's weights, the petrophysical parameters are extrapolated over the seismic segment in the third step.

Multi-linear regression employs log data and seismic as internal attributes and the acoustic impedance produced from inversion as external attributes. Prior to implementing multi-attribute analysis, the saturation log for the well was loaded as the target log and resampled at 2 ms to match the inversion data. The major challenge is determining which group of qualities has the lowest prediction error. Methods of stepwise regression can be utilized to achieve this objective. Ten attributes were used for the hydrate saturation prediction. The top curve in Figure 6.5 represents the training error, whereas the bottom curve represents the validation error.

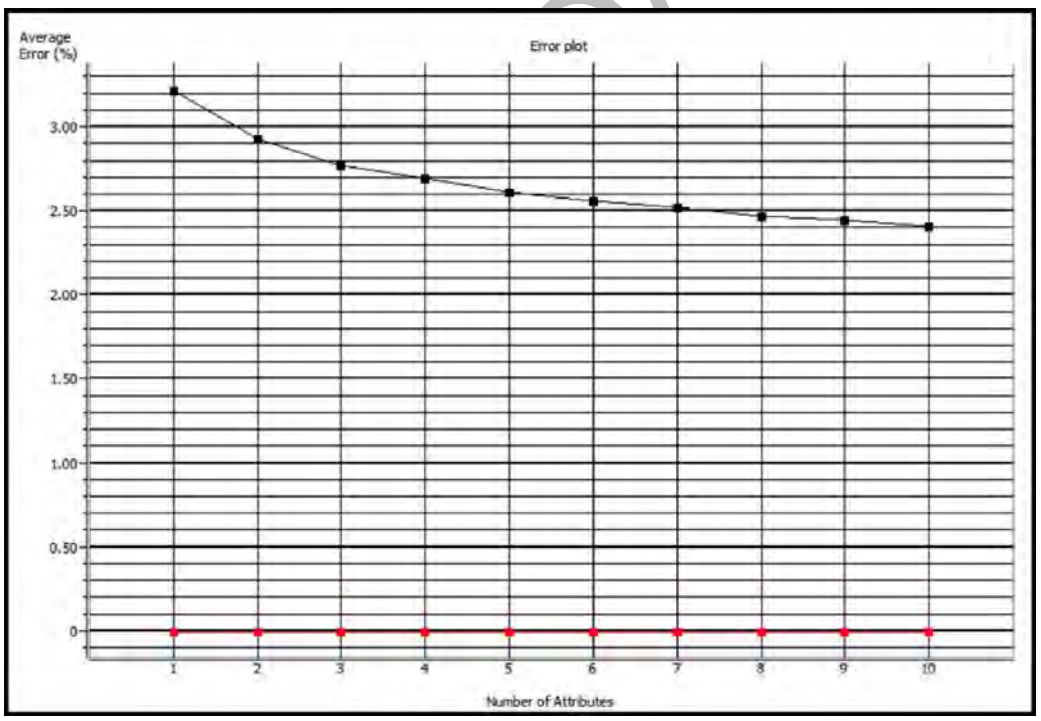

Figure 6.5 Comparison between training and validation errors for hydrate saturation.

Multi-linear attribute regression is applied with the selected ten attributes. The actual saturation log is shown in black, while the predicted log is shown in red, with a correlation coefficient of 0.932 and an error of 1.387%. as shown in figure 6.6.

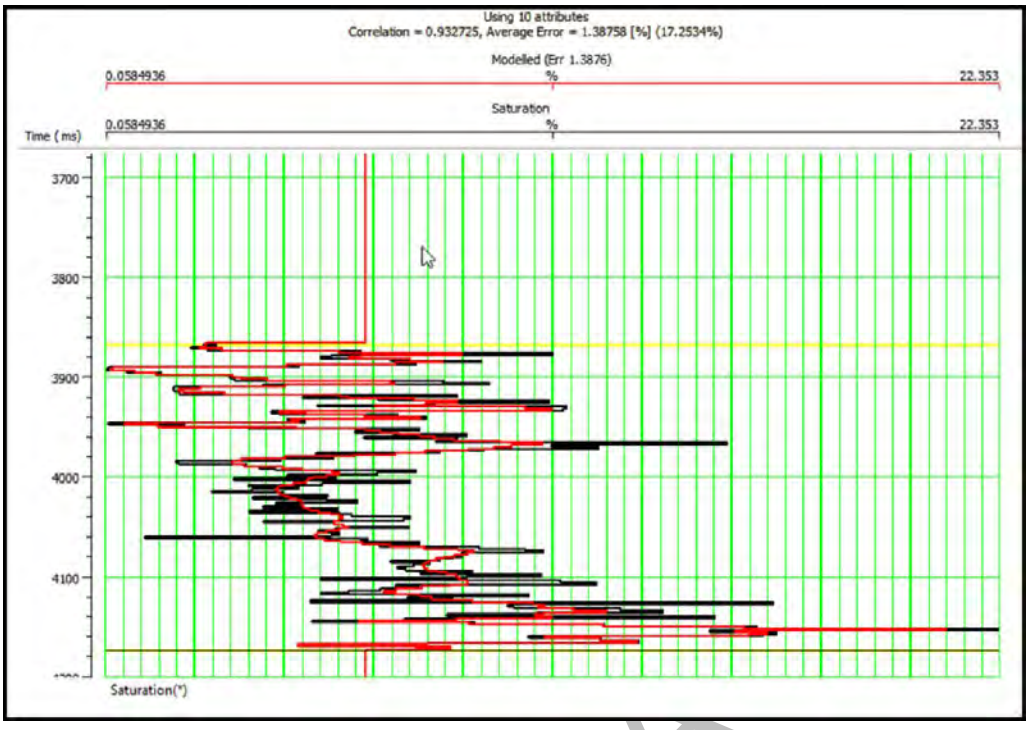

Figure 6.6 Applying the PNN to the well. Red is modeled and black is real saturation curve.

Cross-plots between the actual and predicted petrophysical parameters are created and displayed to examine the quality control of the inverted results in Figure 6.7.

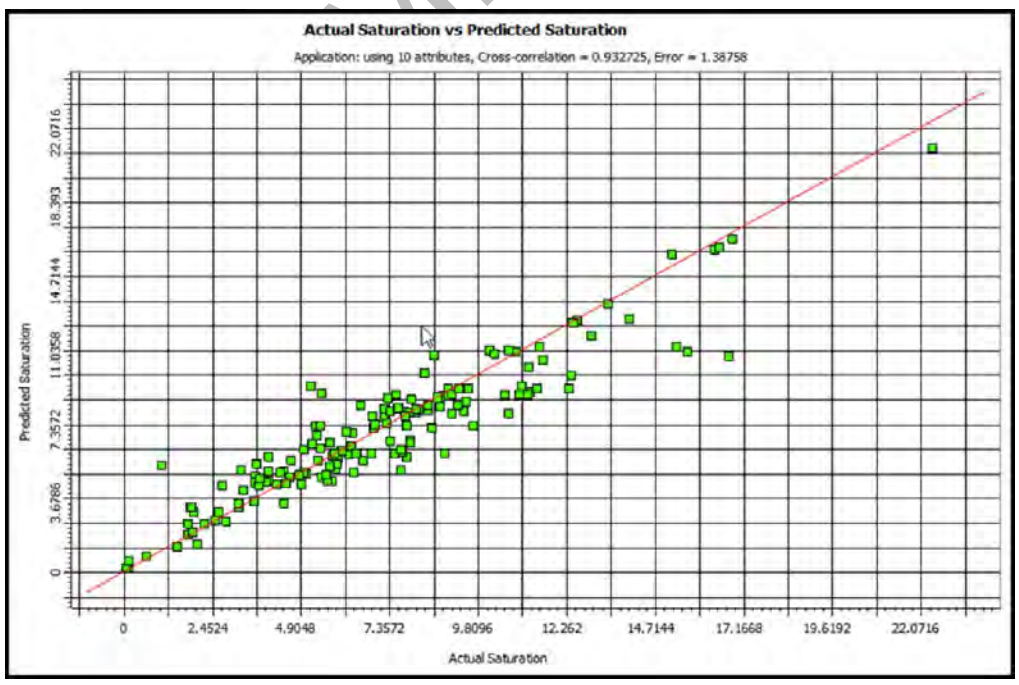

Figure 6.7 A cross-plot between predicted and actual log.

The training window for PNN is 150ms below seabed to Bottom-simulating reflector (BSR) as a target zone. The saturation log placed on the predicted saturation section to show how closely the actual well log curves and the predicted saturation section match (Figure 6.8). It was noticed that the actual saturation log was good match with the predicted seismic section at well location. High saturation of gas hydrates are observed in lower zone of gas hydrates just above the BSR.

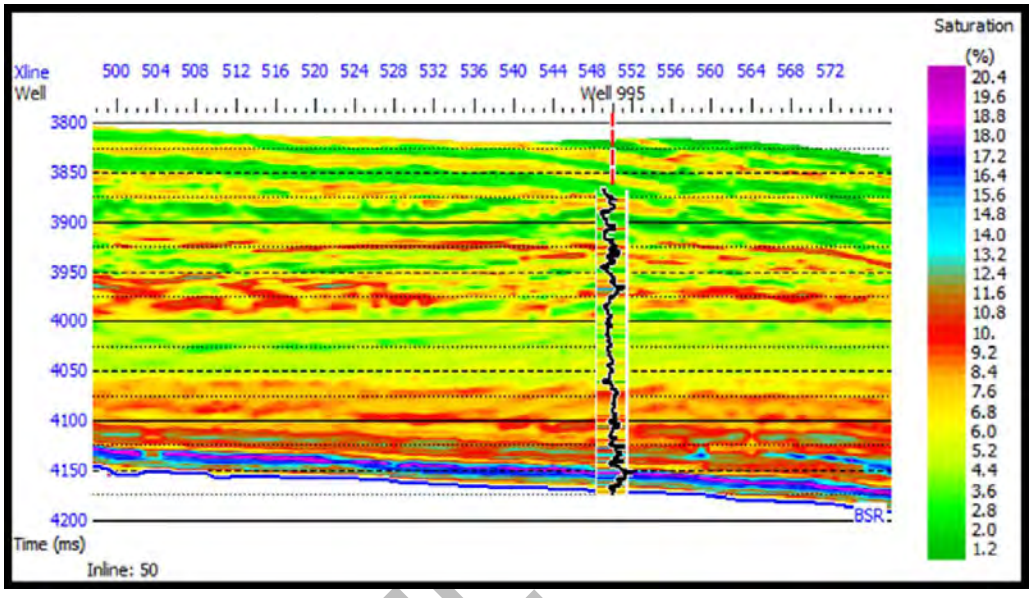

Figure 6.8 Hydrate saturation section for inline 50.

Slice is generated of hydrate saturation above BSR. Type of slice generated is "above target" which is given (BSR-10ms). Slice is of 10ms above this target which is in the lower zone of gas hydrate. Slice is shown in figure 6.9. High percentage of hydrate saturation is present in the area which is confirmed from this slice view of saturation.

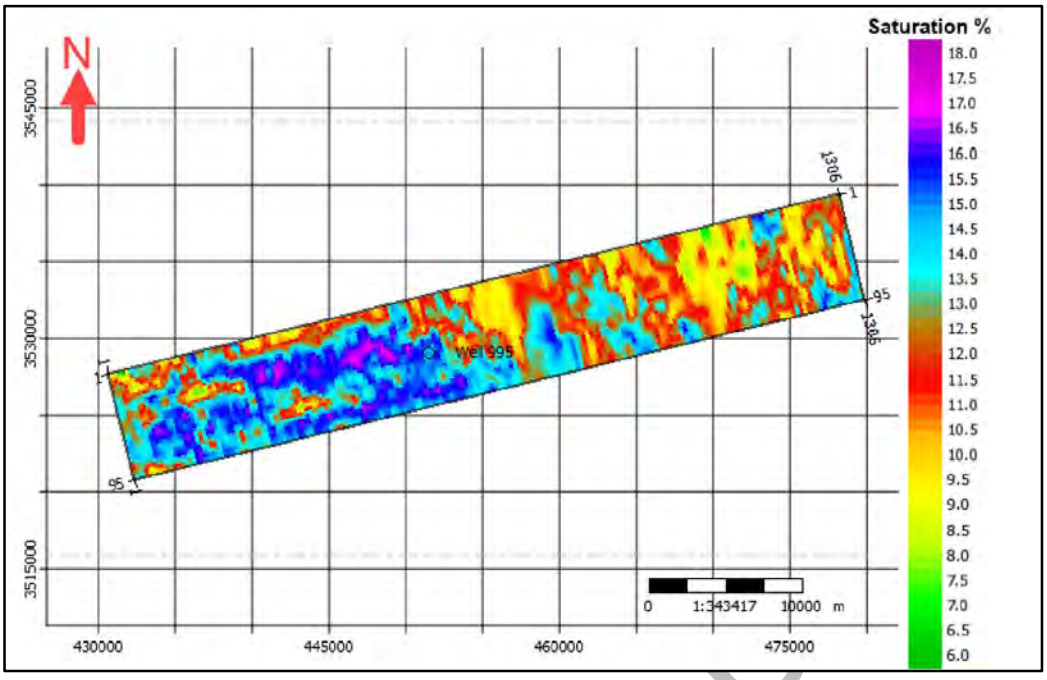

Figure 6.9 Hydrate saturation slice.

Conclusions

- On the seismic, two horizons are marked. First, the seabed or seafloor is the first reflection shown in seismic. Second, BSR is marked with the help of attributes calculated. BSR is not constant throughout the seismic, which could be explained by low methane supply rates or gas seeps.
- Seismic attribute analysis is done on 3D seismic data. Three attributes are applied, which are instantaneous frequency, instantaneous lateral continuity, and trace envelope. These attributes help in marking the bottom-simulating reflector (BSR).
- Amplitude blanking is observed on seismic, which is a typical indication of GHSZ. In GHSZ, there is not a large impedance contrast, so an amplitude blanking phenomenon is observed.
- BSR indicates the free gas zone when gas is present in pores in gaseous form below the GHSZ. This gas accumulation is clearly seen with high impedance contrast on seismic. Attributes also confirm this gas accumulation in the subsurface.
- The results of the petrophysical analysis conclude a suitable environment for the presence of gas hydrates in pore spaces. Low P and S-wave velocities, high porosity values, and low Lambda-Rho and Mu-Rho values support the accumulation of gas hydrates. Average porosity is about 57%. Gas hydrate saturation is also present in pore spaces, with an average value of 6.7%.
- Seismic inversion analysis is done with the help of well data. Model base inversion technique is applied. Inverted P-impedance volume has high impedance values above BSR. S-impedance volume is also calculated and has high S-impedance values above BSR in GHSZ.
- Lambda-Mu-Rho (LMR) is estimated on the seismic scale. Both P-impedance and S-impedance are used for the calculation of LMR. Lambda-Rho and Mu-Rho values are low all along the seismic above BSR.
- Porosity is estimated by the cross-plot method. A correlation above 83% is observed between porosity and P-impedance. The equation from the cross-plot is then used for the estimation of porosity volume. High porosity was observed throughout the data.

- Hydrate saturation is estimated on the seismic scale with the help of probabilistic neural network (PNN). Ten attributes from the seismic are used, and their plot shows low error values. Multi-linear regression with ten attributes shows a good overlay over the actual saturation log with a correlation above 93%. Hydrates can be seen throughout the area in the section and slice.

References

1. Al-Rahim, A. M., & Hashem, H. A. (2016). Subsurface 3D prediction porosity model from converted seismic and well data using Model based inversion technique. *Iraqi Journal of Science*,*57*(1A), 163-174.
2. Aregbe, A. G. (2017). Gas hydrate—properties, formation and benefits. *Open Journal of Yangtze Oil and Gas*, *2*(1), 27-44.
3. Barclay, F., Bruun, A., Rasmussen, K. B., Alfaro, J. C., Cooke, A., Cooke, D., & Roberts, R. (2008). Seismic inversion: Reading between the lines. Oilfield Review, 20(1), 42-63.
4. Brewer, P.G., Orr, F.M., Jr., Friederich, G., Kvenvolden, K.A., Orange, D.L., McFarlane, J., and Kirkwood, W., 1997. Deep-ocean field test of methane hydrate formation from a remotely operated vehicle. Geology, 25:407–410
5. Castagna, J.P., Batzle, M.L., and Eastwood, R.L., 1985. Relationships between compressional-wave and shear-wave velocities in clastic silicate rocks. Geophysics, 50:571–581.
6. Coffeen, J.A., 1986, Seismic Exploration Fundamentals, PennWell Publishing Co.
7. Cooke, D., & Cant, J. (2010). Model-based Seismic Inversion: Comparing deterministic and probabilistic approaches. CSEG Recorder, 28-39.
8. Dillon, L., Schwedersky, G., Vásquez, G., Velloso, R., & Nunes, C. (2003). A multiscale DHI elastic attributes evaluation. *The Leading Edge*, *22*(10), 1024-1029.
9. Dillon, W.P., and Popenoe, P., 1988. The Blake Plateau basin and Carolina Trough. In Sheridan, R.E., and Grow, J.A. (Eds.), The Atlantic Continental Margin, U.S., Geol. Soc. Am., Geology of North America, I-2:291– 328.
10. Dillon, W.P., and Paull, C.K., 1983. Marine gas hydrates, II. Geophysical evidence. In Cox, J.L. (Ed.), Natural Gas Hydrates: Properties, Occurrences, and Recovery: Woburn, MA (Butterworth), 73–90.
11. Dillon, W.P., Lee, M.W., Fehlhaber, K., and Coleman, D.F., 1993. Gas hydrates on the Atlantic margin of the United States—controls on concentration, In Howell, D.G. (Ed.), The Future of Energy Gases. Geol. Surv. Prof. Pap. U.S., 1570:313–330.
12. Dvorkin, J., Nur, A., 1993. Rock Physics for the characterization of gas hydrates, The Future of Energy Gases. USGS Prof. Paper 1570, 293–298.

13. Egeberg, P.K., 2000. Hydrates associated with fluid flow above salt diapirs (site 996), in press
14. Eichkitz, C.G., Amtmann, J., Schreilechner, M.G., 2013. Calculation of grey level cooccurrence matrix-based seismic attributes in three dimensions. Comput. Geosci. 60, 176–183.
15. Esikov, A.D., Pashkina, V., 1990. A study of the process of joint formation of methane gas-hydrate and authigenic carbonates in bottom sediments in the Sea of Okhosk. Natl Geophys. 4 (1), 135–141.
16. Gavotti, P. E. (2014). Model-based inversion of broadband seismic data (Unpublished master's thesis). University of Calgary, Calgary, AB. doi:10.11575/PRISM/26932.
17. Ginsburg, G.D., Soloviev, V.A., 1997. Methane Migration within the submarine gas-hydrate stability zone under deep-water conditions. Mar. Geol. 137, 49–57.
18. Goodway, B., Chen, T., & Downton, J. (1997). Improved AVO fluid detection and lithology discrimination using Lamé petrophysical parameters;"λρ","μρ", & "λ/μ fluid stack", from P and S inversions. In *SEG technical program expanded abstracts 1997* (pp. 183-186). Society of Exploration Geophysicists.
19. Hornbach, Matthew J., Demian M. Saffer, W. Steven Holbrook, Harm J. A. Van Avendonk, and Andrew R. Gorman. "Three-dimensional Seismic Imaging of the Blake Ridge Methane Hydrate Province: Evidence for Large, Concentrated Zones of Gas Hydrate and Morphologically Driven Advection." Journal of Geophysical Research 113.B07101 (2008): 1-15. Print.
20. Haacke, R. Ross, Graham K. Westbrook, and Roy D. Hyndman. "Gas Hydrate, Fluid Flow and Free Gas: Formation of the Bottom-simulating Reflector." Earth and Planetary Science Letters 261.3-4 (2007): 407-20. Web. 29 Feb. 2016.
21. Hampson, D.P., Schuelke, J.S., Quirein, J.A., 2001. Use of multi-attribute transforms to predict log properties from seismic data. Geophysics 66 (1), 220–236.
22. Halleland, K.B., Cotton, J., Hanbal, I., 2007, February. Regional seismic attribute mapping for nile delta deep water reservoir imaging. In: 3rd EAGE North African/ Mediterranean Petroleum and Geosciences Conference and Exhibition. European Association of Geoscientists & Engineers (pp. cp-16).
23. Herrera, V.M., Russell, B., Flores, A., 2006. Neural networks in reservoir characterization. Lead. Edge 25 (4), 402–411.

24. Holbrook, W. Steven, Hartley Hoskins, Warren T. Woods, Ralph A. Stephen, and Daniel Lizarralde. "Methane Hydrate and Free Gas on the Blake Ridge from Vertical Seismic Profiling." Science 273 (1996): n. pag. 17 July 1996. Web. 8 June 2015.
25. Holbrook, W.S., Hoskins, H., Wood, W.T., Stephen, R.A., Lizarralde, D., Leg 164 Science Party, 1996. Methane hydrate and free gas on the blake ridge from vertical seismic profiling. Science 273, 1840–1843.
26. Holvland, M.H., Judd, A.G., 1988. Seabed Pockmarks and Seepages: Impact on Geology, Biology and the Marine Environment, Graham and Trotman, London, 293 pp.
27. Hovland, M.H., 1992. Hydrocarbon seeps in northern marine waters—their occurrence and effects. Palios 7, 376–382
28. Ismail, A., Ewida, H.F., Al-Ibiary, M.G., Gammaldi, S., Zollo, A., 2020c. Identification of gas zones and chimneys using seismic attributes analysis at the Scarab field, offshore, Nile Delta, Egypt. Petrol. Res. 5 (1), 59–69.
29. Ismail, A., Ewida, H.F., Al-Ibiary, M.G., Nazeri, S., Salama, N.S., Gammaldi, S., Zollo, A., 2021. The detection of deep seafloor pockmarks, gas chimneys, and associated features with seafloor seeps using seismic attributes in the West offshore Nile Delta, Egypt. Explor. Geophys. 52 (4), 388–408.
30. Ismail, A., Ewida, H.F., Al-Ibiary, M.G., Zollo, A., 2020b. Integrated prediction of deep water gas channels using seismic coloured inversion and spectral decomposition attribute, West offshore, Nile Delta, Egypt. NRIAG J. Astron. Geophys. 9 (1), 459–470.
31. Kneller, E. A., Albertz, M., Karner, G. D., & Johnson, C. A. (2013). Testing inverse kinematic models of paleocrustal thickness in extensional systems with high-resolution forward thermo-mechanical models. *Geochemistry, Geophysics, Geosystems*, *14*(7), 2383-2398.
32. Kvenvolden, K. A. "A Primer on the Geologic Occurrence of Gas Hydrate. "Gas Hydrates: Relevance to World Margin Stability and Climate Change. N.p.: Geological Society of London, 1998. N. pag. Print.
33. Lee, M. W. 2000. GAS HYDRATES AMOUNT ESTIMATED FROM ACOUSTIC LOGS AT THE BLAKE RIDGE, SITES 994, 995, AND 9971.
34. Lee, M. W., and Dillon, W. P., 2001, Amplitude blanking related to the pore-filling of gas hydrate in sediments: Marine Geophys. Res., 22, 101–109.

35. Lee, M.W., Hutchinson, D.R., Collett, T.S., and Dillon, W.P., 1996. Seismic velocities for hydrate-bearing sediments using weighted equation. J. Geophy. Res., 101:20347–20358.
36. Lee, M.W., Hutchinson, D.R., Dillon, W.P., Miller, J., Agena, W.F., Swift, B.A., 1993. Method of estimating the amount of in situ gas hydrates in deep marine sediments. Marine Petrol. Geol. 10 (5), 493–506.
37. MacKay, M., Westbrook, G., Hyndman, R., ODP Leg 146 Scientific Party, 1994. Origin of bottom simulating reflectors: geophysical evidence from the Cascadia accretionary prism. Geology 22, 459–462.
38. Matsumoto R (1995) Causes of the $\delta^{13}C$ anomalies of carbonates and a new paradigm 'Gas Hydrate Hypothesis'. Journal of the Geological Society of Japan 101: 902}924 (in Japanese with English abstract).
39. McQuillin, R., Bacon, M., and Barclay, W., 1984. An introduction to seismic interpretation, Graham & Trotman Limited Sterling House, 66 Wilton Road London
40. Mohamed, I.A., Hemdan, M., Hosny, A., Rashidy, M., 2019. High resolution water saturation prediction using geostatistical inversion and neural network methods. Interpretation 7 (2), T455–T465.
41. Mohamed, I.A., Shenkar, O., Mahmoud, H., 2017. Understanding reservoir heterogeneity through water-saturation prediction via neural network—a case study from offshore Nile Delta. Lead. Edge 36 (4), 298–303.
42. Monier, D., El Rawy, A., Mahmoud, A., 2021. Delineation of reservoir channels by different seismic attributes and geobody extractions for robust volumetric estimation, Saffron Field, offshore Nile Delta, Egypt. Lead. Edge 40 (7), 484–493.
43. Othman, A.A., Fathy, M., Negm, A., 2018. Identification of channel geometries applying seismic attributes and spectral decomposition techniques, Temsah Field, Offshore East Nile Delta, Egypt. NRIAG J. Astron. Geophys. 7 (1), 52–61.
44. Paull, C.K., Matsumoto, R., Wallace, P.J., et al., 1996. Proc. ODP, Init. Repts., 164: College Station, TX (Ocean Drilling Program).
45. Paull, C.K., Spiess, F.N., Ussler III, W., Borowski, W.S., 1995. Methane-rich plumes on the Carolina continental rise: associations with gas hydrates. Geology 23, 89–92.

46. Pearson, C.F., Halleck, P.M., McGuire, P.L., Hermes, R., and Mathews, M., 1983. Natural gas hydrate deposits: a review of in-situ properties. J. Phys. Chem., 87:4180–4185.
47. Ray, A. K., & Chopra, S. (2016). Building more robust low-frequency models for seismic impedance inversion. *First Break*, *34*(5).
48. Rempel, A. W., & Buffett, B. A. (1997). Formation and accumulation of gas hydrate in porous media. *Journal of Geophysical Research: Solid Earth*, *102*(B5), 10151-10164.
49. Rider, M. H. (1986). The geological interpretation of well logs.
50. Ruffine, L., Donval, J. P., Charlou, J. L., Cremière, A., & Zehnder, B. H. (2010). Experimental study of gas hydrate formation and destabilisation using a novel high-pressure apparatus. *Marine and Petroleum Geology*, *27*(6), 1157-1165.
51. Ruppel, C., 1997. Anomalously cold temperatures observed at the base of the gas hydrate stability zone on the U.S. Atlantic passive margin. Geology, 25:699–702.
52. Russell, B. 1988. Introduction to Seismic Inversion Methods. Society of Exploration Geophysicists
53. Russell, B. H., Hedlin, K., Hilterman, F. J., & Lines, L. R. (2003). Fluid-property discrimination with AVO: A Biot-Gassmann perspective. *Geophysics*, *68*(1), 29-39.
54. Sarhan, M.A., Safa, M.G., 2017. Application of seismic attributes for detecting different geologic features within kafr El sheikh formation, temsah concession, nile delta basin. Sci. J. Damietta Fac. Sci. 7 (1), 26–34.
55. Sen, M. K. (2006). Seismic inversion. Richardson, TX.: Society of Petroleum Engineers.
56. Sloan, E.D., 1990. Clathrate Hydrates of Natural Gases: New York (Marcel Dekker).
57. Soloviev, V.A., Ginsburg, G.D., 1997. Water segregation in the course of gas hydrate formation and accumulation in submarine gas-seepage fields. Mar. Geol. 137, 59–68.
58. Subrahmanyam, D., Rao, P.H., 2008, January. Seismic attributes-A review. In: 7th International Conference & Exposition on Petroleum Geophysics, pp. 398–404. Hyderabad.
59. Taner, M. T., F. Koehler, and R. E. Sheriff, 1979, Complex seismic trace analysis: Geophysics, 44, 1041–1063.

60. Telford, W.M., Geldart, L.P., Sheriff, R.E., and Keys, D.A., 1999, Applied Geophysics, Cambridge University Press, London.
61. Timur, A, 1968. Velocity of compressional waves in porous media at permafrost temperature. Geophysics, 33:584–595.
62. Tinivella, Umberta, and Emanuele Lodolo. "The Blake Ridge Bottom-simulating Reflector Transect: Tomographic Velocity Field and Theoretical Model to Estimate Methane Hydrate Quantities."Proceedings of the Ocean Drilling Program Proceedings of the Ocean Drilling Program, 164 Scientific Results (2000): n. pag. Web. 29 Feb. 2016.
63. Tinivella, Umberta, and F. Accaino. "Compressional Velocity Structure and Poisson's Ratio in Marine Sediments with Gas Hydrate and Free Gas by Inversion of Reflected and Refracted Seismic Data (South Shetland Islands, Antarctica)." Marine Geology, 2000. Web. 29 Feb. 2016.
64. Todorov, T.I., 2000. Integration of 3C-3D Seismic Data and Well Logs for Rock Property Estimation. University of Calgary. M.S. thesis.
65. Tohidi, B. (2014) Advances in Avoiding Gas Hydrate Problems. Centre for Gas Hydrate Research & Hydrafact Ltd., Institute of Petroleum Engineering, Heriot-Watt University, 1-47.
66. Tonn, R., 2002. Neural network seismic reservoir characterization in a heavy oil reservoir. Lead. Edge 21 (3), 309–312.
67. Tucholke, B.E., Bryan, G.M., and Ewing, J.I., 1977. Gas hydrate horizon detected in seismic reflection profiler data from the western North Atlantic. AAPG Bull., 61:698-707.
68. Waite, W.F., Helgerud, M.B., Nur, A., Pinkston, J., Stern, L.A., Kirby, S.H., Durham, W.B., 1998. EOS Transactions, vol. 79(45). American Geophysical Union, p. 463.
69. Wood, A.B., 1941. A Textbook of Sound (2nd ed.): New York (MacMillan).
70. Yilmaz, O., 1987. Seismic Data Processing; Investigations in Geophysics. Society of Exploration Geophysicists. Tulsa, vol. 2, 526 pp.